JEM Journal of Experimental Medicine

ARTICLE

# Neutrophil DREAM promotes neutrophil recruitment in vascular inflammation

Jing Li[1*], Tripti Kumari[2*], Andrew Barazia[1*], Vishwanath Jha[2], Si-Yeon Jeong[1], Amber Olson[2], Mijeong Kim[3], Bum-Kyu Lee[3], Vijayprakash Manickam[2], Zhimin Song[4,5], Regina Clemens[4,5], Babak Razani[5,6,7], Jonghwan Kim[3], Mary C. Dinauer[4,5], and Jaehyung Cho[1,2,5]

**The interaction between neutrophils and endothelial cells is critical for the pathogenesis of vascular inflammation. However, the regulation of neutrophil adhesive function remains not fully understood. Intravital microscopy demonstrates that neutrophil DREAM promotes neutrophil recruitment to sites of inflammation induced by TNF-α but not MIP-2 or fMLP. We observe that neutrophil DREAM represses expression of A20, a negative regulator of NF-κB activity, and enhances expression of pro-inflammatory molecules and phosphorylation of IκB kinase (IKK) after TNF-α stimulation. Studies using genetic and pharmacologic approaches reveal that DREAM deficiency and IKKβ inhibition significantly diminish the ligand-binding activity of β2 integrins in TNF-α–stimulated neutrophils or neutrophil-like HL-60 cells. Neutrophil DREAM promotes degranulation through IKKβ-mediated SNAP-23 phosphorylation. Using sickle cell disease mice lacking DREAM, we show that hematopoietic DREAM promotes vaso-occlusive events in microvessels following TNF-α challenge. Our study provides evidence that targeting DREAM might be a novel therapeutic strategy to reduce excessive neutrophil recruitment in inflammatory diseases.**

## Introduction

In addition to the host defense function against bacterial infection, neutrophils play a crucial role in the pathophysiology of sterile inflammation (Linnerz and Hall, 2020; Phillipson and Kubes, 2011). However, excessive neutrophil recruitment to sites of inflammation causes severe tissue damage. Neutrophil recruitment initiated by rolling on activated endothelial cells (ECs) through interactions between P-/E-selectins and their ligands, including P-selectin glycoprotein ligand-1 (PSGL-1; Phillipson and Kubes, 2011). Subsequently, activated integrins, mainly αLβ2 and αMβ2, bind to their ligands, such as intercellular adhesion molecule-1 (ICAM-1), and mediate slow rolling, adhesion, and crawling of neutrophils. In the presence of chemoattractants, crawling neutrophils transmigrate across the EC barrier, killing bacteria or inducing tissue damage. In addition, adherent neutrophils can support platelet adhesion and microthrombus formation, leading to microvascular occlusion and aggravating inflammatory conditions (Kim et al., 2015; Li et al., 2014; Li et al., 2019). Because of the critical roles in neutrophil recruitment, selectins and integrins have been targeted for the treatment of inflammatory diseases (Arnaout, 2016; Ataga et al., 2017; McEver, 2015). Complete blockade of leukocyte–EC contact, however, could impair immune responses (Wolf et al., 2018). Therefore, a better understanding of neutrophil–EC interactions would provide insights into more nuanced therapeutic strategies that block excessive neutrophil recruitment under inflammatory conditions.

Downstream regulatory element antagonist modulator (DREAM), a transcriptional repressor, regulates various cellular functions, including gene transcription, apoptosis, and protein folding (Calì et al., 2012; Craig et al., 2013; Mellström et al., 2014). The first study of DREAM KO mice showed that DREAM controls the expression of prodynorphin mRNA and dynorphin A peptides in the spinal cord and modulates pain responses (Cheng et al., 2002). During cell activation, DREAM binds to $Ca^{2+}$ and is dissociated from the DRE motif, allowing gene transcription (Mellström et al., 2014). In ECs, DREAM binds to DRE3 and DRE4

[1]Department of Pharmacology, University of Illinois at Chicago College of Medicine, Chicago, IL; [2]Division of Hematology, Department of Medicine, Washington University School of Medicine, St. Louis, MO; [3]Department of Molecular Biosciences, University of Texas at Austin, Austin, TX; [4]Department of Pediatrics, Washington University School of Medicine, St. Louis, MO; [5]Department of Pathology and Immunology, Washington University School of Medicine, St. Louis, MO; [6]Cardiovascular Division, Department of Medicine, Washington University School of Medicine, St. Louis, MO; [7]John Cochran VA Medical Center, St. Louis, MO.

*J. Li, T. Kumari, and A. Barazia contributed equally to this paper; Correspondence to Jaehyung Cho: jaehyung.cho@wustl.edu; A. Barazia's present address is Intelligent Imaging Innovations, Denver, CO; B.K. Lee's present address is Department of Biomedical Sciences, Cancer Research Center, University at Albany–State University of New York, Rensselaer, NY; S.Y. Jeong's present address is Division of Pharmaceutical Policy, Pharmaceutical Safety Bureau, Ministry of Food and Drug Safety, Cheongju-si, South Korea.

in the promoter of the *TNFAIP3* gene encoding A20, a negative regulator of NF-κB signaling, and represses its expression, enhancing NF-κB activity during LPS-induced acute lung injury (Tiruppathi et al., 2014). In addition to its binding to DNA, DREAM interacts with numerous proteins, including calmodulin and presenilin (Buxbaum et al., 1998; Gonzalez et al., 2015). We also demonstrated that platelet DREAM nontranscriptionally enhances platelet activation and arterial thrombosis by regulating activation of class Iβ phosphoinositide 3-kinase (Kim et al., 2017b). However, it is unknown whether neutrophil DREAM plays a role in vascular disease.

The NF-κB family consists of five transcription factors: p50, p52, p65, RelB, and c-Rel. By forming homodimers or heterodimers, these transcription factors share an N-terminal DNA-binding and dimerization domain and induce the expression of many pro-inflammatory genes (Li and Verma, 2002). Under normal conditions, the NF-κB complex binds to IκB and is sequestered in the cytoplasm. Following stimulation with TNF-α, IκB kinase (IKK) is activated via TNF receptor–associated factors (TRAFs) and TNF-α–activated kinases, such as receptor-interacting protein kinases (RIPKs; Cabal-Hierro and Lazo, 2012). Activated IKK phosphorylates IκB, leading to its ubiquitination and proteasomal degradation. A20 is a potent anti-inflammatory protein that inhibits TRAFs and RIPK1 by regulating ubiquitination and impairs IKK activation via a noncatalytic mechanism (Boone et al., 2004; Skaug et al., 2011; Wertz et al., 2004). The NF-κB complex dissociated from IκB translocates into the nucleus and binds to consensus sites in the DNA of target genes (Hayden and Ghosh, 2011). Although EC DREAM promotes NF-κB–induced gene transcription (Tiruppathi et al., 2014), the role of neutrophil DREAM in inflammation remains unknown.

In the present study, we demonstrate that neutrophil DREAM enhances neutrophil adhesive function in vascular inflammation via NF-κB–dependent and –independent mechanisms. Neutrophil DREAM positively regulates neutrophil recruitment to sites of vascular inflammation induced by TNF-α but not macrophage inflammatory protein-2 (MIP-2) or fMLP. Deletion of neutrophil DREAM down-regulates the expression of pro-inflammatory cytokines and up-regulates anti-inflammatory molecules following TNF-α stimulation. Furthermore, neutrophil DREAM positively regulates the ligand-binding activity of β2 integrins and degranulation through activated IKK after short-term treatment with TNF-α in an NF-κB–independent manner. In vivo studies using sickle cell disease (SCD) mice reveal that deletion of hematopoietic DREAM attenuates intravascular cell–cell aggregation and improves the survival of TNF-α–challenged SCD mice. These results suggest that targeting DREAM might be a novel therapeutic strategy to reduce excessive neutrophil recruitment in vascular inflammation.

## Results

### DREAM positively regulates neutrophil recruitment during vascular inflammation induced by TNF-α but not MIP-2 or fMLP

To study the role of DREAM in vascular inflammation, we performed intravital microscopy on DREAM KO mice. Deletion of DREAM significantly increased the number of rolling neutrophils and markedly enhanced the rolling velocity on the TNF-α–inflamed cremaster venular wall (Fig. 1, A–C; Video 1; and Video 2). The numbers of adherent and transmigrated neutrophils and the percentage of crawling neutrophils were lower in DREAM KO mice than WT mice (Fig. 1, D–F). As reported previously (Kim et al., 2017b), no significant difference in blood counts was observed between WT and DREAM KO mice (Table S1). Loss of DREAM moderately but significantly increased the blood flow rate in the cremaster venules in TNF-α–challenged mice (Table 1).

To further investigate whether DREAM contributes to neutrophil recruitment in chemoattractant-induced vascular inflammation, intravital microscopy was performed with mice treated with intrascrotal injection of MIP-2 (Fig. 1, G–I) or superfusion of fMLP (Fig. 1, J–M). Compared with WT mice, DREAM KO mice did not show any defects in neutrophil rolling, adhesion, and transmigration. These results suggest that DREAM promotes neutrophil recruitment to sites of vascular inflammation induced by TNF-α but not MIP-2 or fMLP.

### Neutrophil DREAM contributes to neutrophil recruitment during TNF-α–induced vascular inflammation

To determine the relative contributions of hematopoietic and nonhematopoietic DREAM to neutrophil recruitment in vascular inflammation, we performed intravital microscopy on chimeric mice generated by transplantation of bone marrow (BM) cells from WT and DREAM KO mice into irradiated WT and KO mice. Compared with WT-BM → WT mice, WT-BM → KO, KO-BM → WT, and KO-BM → KO mice exhibited a significantly greater rolling number and velocity of neutrophils on the TNF-α–inflamed endothelium (Fig. 2, A–C). The number of adherent neutrophils was decreased by loss of nonhematopoietic or hematopoietic DREAM, or both (Fig. 2 D). Neutrophil crawling was also impaired in WT-BM → KO, KO-BM → WT, or KO-BM → KO mice compared with WT-BM → WT mice (Fig. 2 E). Intriguingly, no differences in neutrophil rolling, adhesion, and crawling were observed between either WT-BM → KO or KO-BM → WT mice and KO-BM → KO mice, implying that the interaction between a neutrophil receptor and its EC counter receptor is reduced by DREAM deletion. Consistent with our previous finding (Kim et al., 2017b), no difference was observed in blood counts in the four groups (Table S2). DREAM deficiency in either hematopoietic or nonhematopoietic cells or both enhanced blood flow rates in the inflamed venules (Table 2). These results indicate that both hematopoietic and nonhematopoietic DREAM play roles in neutrophil–EC interactions in vascular inflammation.

EC DREAM has been reported to enhance NF-κB activity in LPS-induced acute lung injury (Tiruppathi et al., 2014), and TNF-α signaling activates NF-κB (Hayden and Ghosh, 2011). Thus, we investigated whether DREAM regulates the expression of adhesion molecules in the TNF-α–inflamed endothelium. As assessed by immunohistochemistry with TNF-α–inflamed cremaster endothelium, we found that ICAM-1 expression was significantly down-regulated in WT-BM → KO and KO-BM → KO mice compared with WT-BM → WT and KO-BM → WT mice (Fig. 2 F). However, the expression of E-selectin and P-selectin

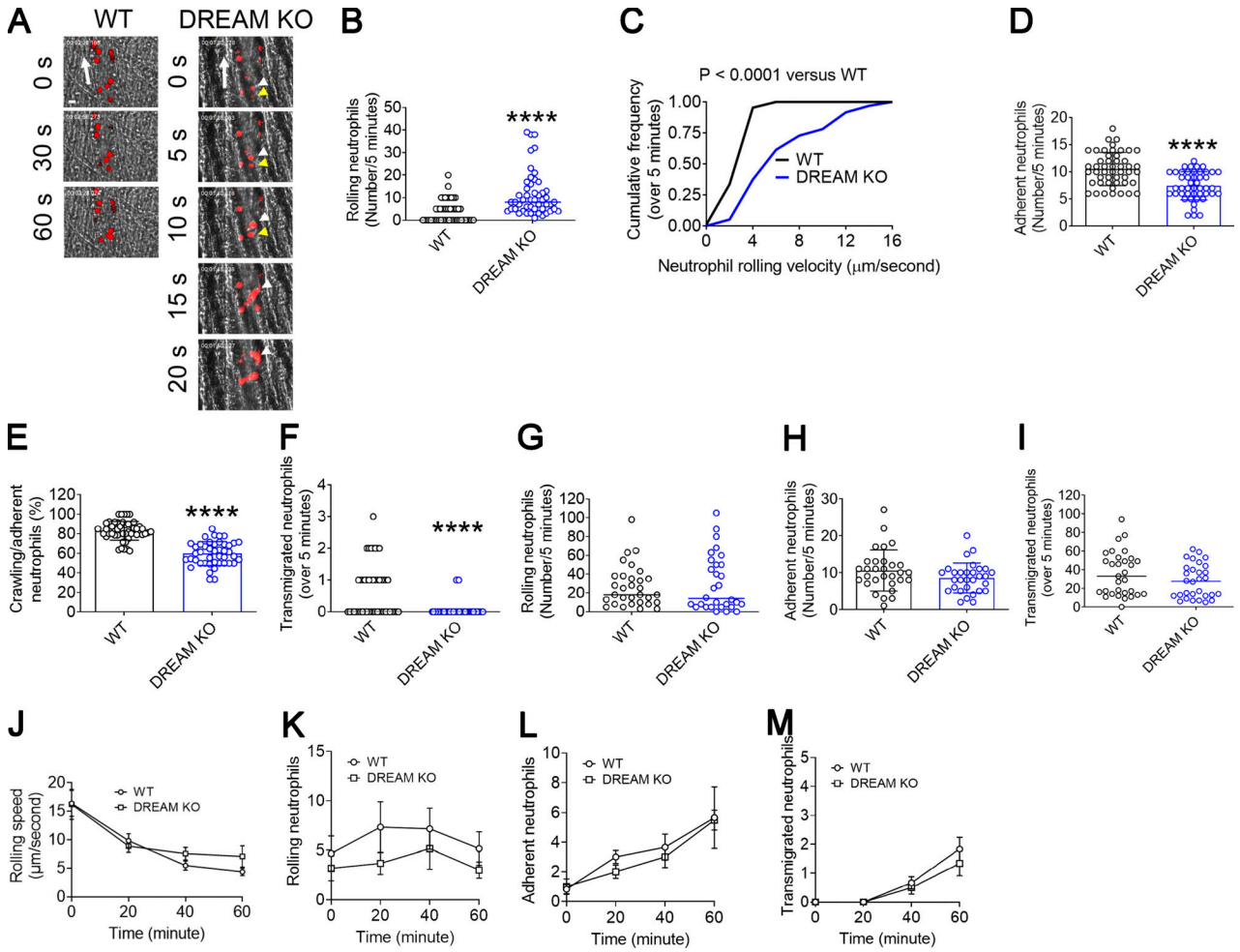


Figure 1. **Neutrophil DREAM plays a positive role in neutrophil recruitment in TNF-α–induced vascular inflammation. (A–F)** Intravital microscopy of WT and DREAM KO mice was performed as described in the Materials and methods. Vascular inflammation was induced by intrascrotal injection of TNF-α. 3 h later, rolling, adherent, crawling, and transmigrated neutrophils were visualized in the cremaster venules by infusion of an Alexa Fluor 647–conjugated anti–Ly-6G antibody. The numbers of rolling, adherent, and transmigrated neutrophils were counted in each vessel for 5 min and normalized to the vessel length. **(A)** Representative images. "0" was set when image capture began on each vessel. Large arrows indicate the direction of blood flow. Colored arrowheads indicate individual rolling neutrophils over 20 s. Scale bar = 10 μm. **(B)** The rolling number of neutrophils. **(C)** The cumulative frequency of the rolling velocity of neutrophils. **(D and E)** The number of adherent neutrophils and the percentage of crawling cells among adherent neutrophils. **(F)** The number of transmigrated neutrophils in the field of view (0.02 $mm^2$). **(G–I)** Vascular inflammation was induced by intrascrotal injection of MIP-2. 2 h later, neutrophil recruitment was evaluated as described above. The numbers of rolling (G), adherent (H), and transmigrated neutrophils (I). **(J–M)** Neutrophil recruitment was induced by superfusion with 10 μM fMLP at 37°C for 20, 40, and 60 min. The first capture before fMLP superfusion is shown as time 0. **(J)** The rolling speed and the numbers of rolling (K), adherent (L), and transmigrated neutrophils (M) were determined during a 5-min recording period. The horizontal bar represents the median value in B, F, G, and I. Otherwise, data represent the mean ± SD ($n$ = 46–49 venules in seven mice/group for A–F, $n$ = 30 venules in three mice/group for G–I, and $n$ = 3 mice/group for J–M). ****, P < 0.0001 versus WT control after Student's $t$ test (D, E, H, and J–M) or Mann–Whitney $U$ test (B, C, F, G, and I).

was not altered by DREAM deficiency (Fig. 2 G and Fig. S1). These results suggest that EC DREAM regulates the expression of some, but not all, adhesion molecules, such as ICAM-1, and promotes neutrophil adhesion to the TNF-α–inflamed endothelium.

To further determine whether neutrophil DREAM regulates neutrophil adhesive function, we adoptively transferred isolated WT or DREAM KO neutrophils into TNF-α–challenged WT or DREAM KO mice and examined their intrinsic capacity to roll on and adhere to inflamed endothelium. Compared with WT neutrophils, DREAM KO neutrophils exhibited increased rolling and decreased adhesion when injected into WT mice (Fig. 2, H and I). Neutrophil rolling and adhesion were also impaired when WT neutrophils were injected into DREAM KO mice. The adhesion defect in DREAM KO neutrophils was similar in WT and DREAM KO mice, suggesting that neutrophil and EC DREAM are likely to regulate the function of a neutrophil receptor and its EC counter-receptor.

Although the adoptive transfer experiments suggest a cell-autonomous role of DREAM in neutrophil recruitment, the defect might have been derived from a different environment during neutrophil development. To rule out this possibility, we generated BM chimeric mice with both WT (CD45.1) and DREAM KO (CD45.2) hematopoietic cells. We confirmed that the blood cells in the chimeric mice were equally derived from WT and KO cells (Fig. 2, J–M) at 6 wk after transplantation of an

Table 1. **The hemodynamic parameters in TNF-α–challenged WT and DREAM KO mice**

| Genotype | WBC (cells/μl) | % of neutrophils | Diameter of venules (μm) | Blood flow rate ($\mu l^{-6}/s$) |
|---|---|---|---|---|
| WT | 3,100 ± 750 | 39 ± 6 | 33.5 ± 4 | 426 ± 105 |
| DREAM KO | 4,300 ± 1,220 | 45 ± 9 | 35.2 ± 4 | 652 ± 129* |

Mice were treated with intrascrotal injection of TNF-α, followed by intravital microscopy as described in Fig. 1. After 1 h imaging, fluorescently labeled microspheres (diameter: 200 nm) were injected into mice, and the centerline velocity was calculated to assess blood flow rates. Data represent the mean ± SD ($n$ = 12 venules in 6 mice per group). *, $P < 0.05$ versus WT mice after Student's $t$ test. WBC, white blood cells.

equal number of WT and KO BM cells into irradiated WT (CD45.1) mice. Furthermore, the numbers of all blood cells in the chimeric mice were within a normal range (Table 3). Using intravital microscopy, we found that compared with WT neutrophils ($CD45.1^+/Ly\text{-}6G^+$), DREAM KO neutrophils ($CD45.2^+/Ly\text{-}6G^+$) exhibited a significantly greater rolling number and velocity on the TNF-α–inflamed venular endothelium (Fig. 2, N–P; and Video 3). The number of adherent and transmigrated neutrophils was decreased by DREAM deletion (Fig. 2, Q and R). These results further support a cell-autonomous contribution of neutrophil DREAM to neutrophil recruitment.

Furthermore, we performed flow chamber assays under a venous shear of 1 dyne/$cm^2$. When WT and DREAM KO neutrophils were pretreated with TNF-α and perfused over a monolayer of TNF-α–stimulated mouse pulmonary vein ECs, KO cells showed greater rolling and less adhesion and transmigration than WT cells (Fig. 2, S–W; Video 4; and Video 5). When neutrophils were pretreated with fMLP, these defects were not observed (Fig. 2, U–W). Taken together, our results indicate that neutrophil DREAM positively regulates neutrophil adhesive function in vascular inflammation via the TNF-α signaling pathway.

### Neutrophil DREAM positively regulates NF-κB signaling

Since neutrophil DREAM appears to be important for TNF-α signaling, we first conducted chemokine arrays using 25 different chemokine antibodies to examine whether DREAM is involved in chemokine production in TNF-α–stimulated neutrophils. In a control experiment, we confirmed that the purity of mouse BM-derived neutrophils was 89%, and neutrophil doublets (6.3%) and a minimal number of monocytes ($Ly6G^-/Ly6C^+$) and $CD19^+$ lymphocytes (1.2%) were present (Fig. S2 A). As normalized to loading controls (gp130 and Hsp60), CXCL2 and CXCL10 were significantly up-regulated in TNF-α–stimulated neutrophils, but no significant difference was observed between WT and DREAM KO neutrophils (Fig. 3 A).

To further evaluate DREAM-regulated gene expression, we treated WT and DREAM KO neutrophils with TNF-α and analyzed their transcriptomic profiles by RNA sequencing (RNA-seq). Gene set enrichment analysis (GSEA) revealed that deletion of neutrophil DREAM down-regulated genes involved in pro-inflammatory responses, such as *Il-6*, *Il-16*, and *Il-17rb*, but up-regulated genes associated with anti-inflammatory responses, such as *Fpr2*, *Tnfaip6*, and *Tnfaip3* at 30 min after TNF-α treatment (Fig. 3 B, Table S3, and Gene Expression Omnibus accession no. GSE172394). The differences, however, were less remarkable or not observed after treatment with TNF-α for 120 min (Table S3). Since *Tnfaip3* encodes A20, a negative regulator of NF-κB signaling (Wertz et al., 2004), these results suggest that neutrophil DREAM might play a role in NF-κB signaling.

We found that A20 expression was up-regulated in DREAM KO neutrophils compared with WT neutrophils, and remained elevated for 3 h after TNF-α stimulation (Fig. 3 C). Pro–IL-1β expression was lower in TNF-α–stimulated KO neutrophils than WT neutrophils (Fig. 3 C). DREAM expression remained unchanged in WT neutrophils after TNF-α stimulation, and the expression of αM, β2, p65, and p50 was not altered by DREAM deletion. DREAM deletion did not affect neutrophil apoptosis induced by TNF-α (Fig. 3 D). Since DREAM binds to the DRE sites in the promoter of the *Tnfaip3* gene encoding A20 in ECs (Tiruppathi et al., 2014), chromatin immunoprecipitation (ChIP) was performed with quantitative PCR (qPCR). We observed that neutrophil DREAM bound to the promoter region (DRE1-2) of *Tnfaip3* (Fig. 3, E and F), suggesting that neutrophil DREAM represses A20 expression transcriptionally and promotes NF-κB–induced pro-inflammatory gene transcription.

IKK controls NF-κB activity, and phosphorylation of Ser176/Ser180 in IKKα and Ser177/Ser181 in IKKβ is critical for their kinase activity (Ling et al., 1998; Mercurio et al., 1997). We observed that compared with WT neutrophils, DREAM KO neutrophils exhibited a significant reduction in IKKα/β phosphorylation after stimulation with 5–20 ng/ml TNF-α (Fig. 3 G and data not shown). Consistent with this finding, loss of DREAM impaired IκB degradation after TNF-α stimulation, along with increased A20 expression (Fig. 3 H). These results suggest that neutrophil DREAM is important for TNF-α–induced IKK activation.

Because of the lack of DREAM inhibitors, we used shRNA to knock down the *KCNIP3* gene encoding DREAM in HL-60 cells, which have similar morphological and functional characteristics to human neutrophils after differentiation (Xu et al., 2003). In control experiments, we confirmed that isolated human blood neutrophils expressed DREAM mRNA and protein (Fig. S2 B; and Fig. 3, I and J). Compared with scrambled shRNA, DREAM shRNA#1 and #4 significantly reduced the expression of DREAM protein in differentiated HL-60 (dHL-60) cells (Fig. 3 K). shRNA-mediated knockdown of DREAM up-regulated A20 expression without affecting the expression of other proteins, such as αM, β2, p65, and p50 (Fig. 3 L), and inhibited TNF-α–induced IκB degradation (Fig. 3 M). These results corroborate our findings in

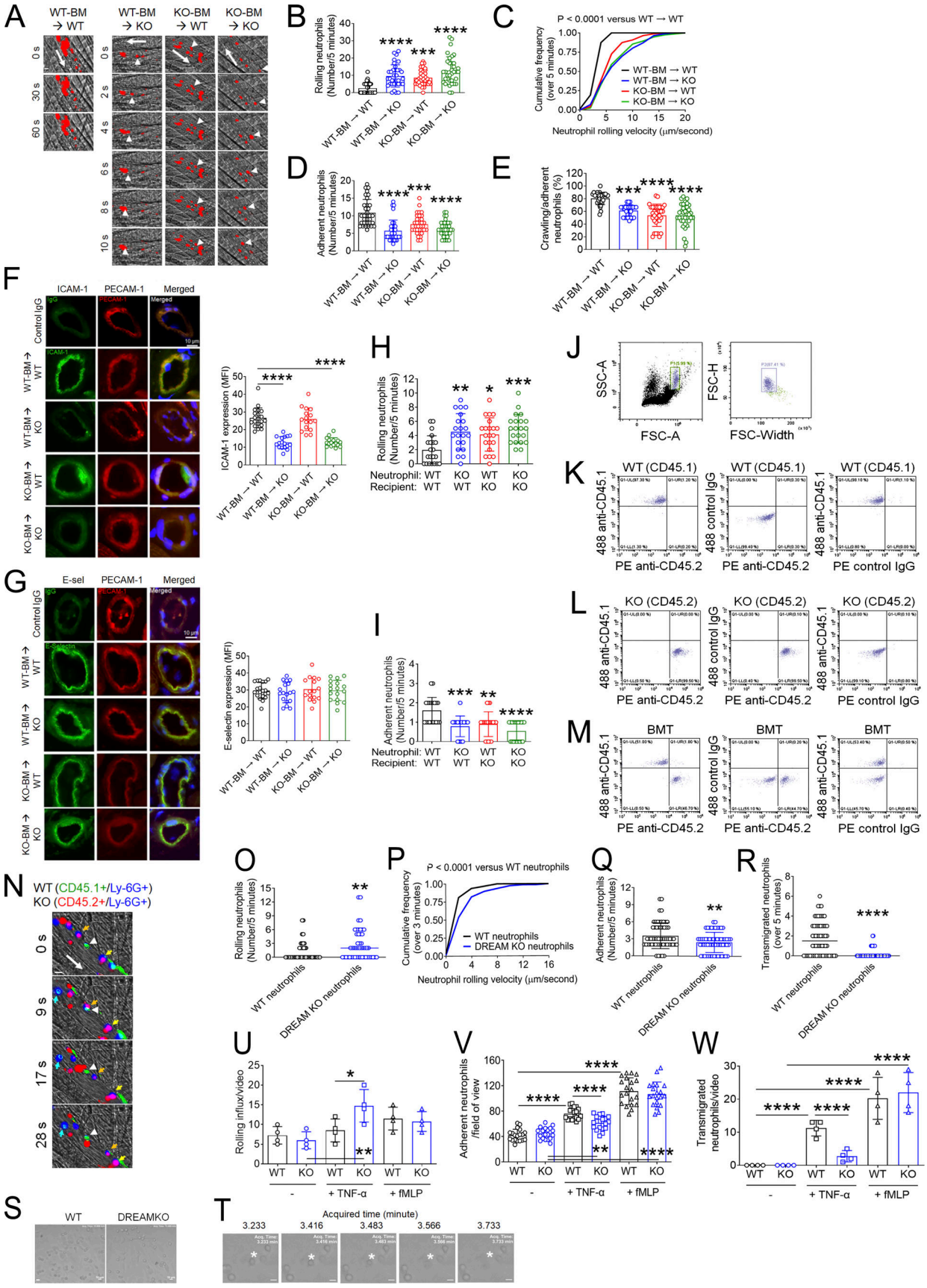


Figure 2. **Neutrophil DREAM contributes to neutrophil recruitment during TNF-α–induced vascular inflammation.** Intravital microscopy with BM chimeric mice was performed as described in Fig. 1. **(A)** Representative images. Large arrows indicate the direction of blood flow. Arrowheads indicate

individual rolling neutrophils over 10 s. **(B)** The rolling number of neutrophils. **(C)** The cumulative frequency of the rolling velocity of neutrophils. **(D and E)** The number of adherent neutrophils and the percentage of crawling neutrophils. Data represent the mean ± SD ($n$ = 36–39 venules in six mice/group). **(F and G)** After intravital microscopy, the cremaster muscle in each mouse was removed and sectioned for immunohistochemistry. Tissue sections were stained for ICAM-1, E-selectin (E-sel), PECAM-1, and DAPI, and used for confocal microscopy. The MFI values of anti–ICAM-1 and anti–E-selectin antibodies were quantified. Data represent the mean ± SD ($n$ = 20 sections in four mice/group). **(H and I)** Fluorescently labeled WT and DREAM KO neutrophils were adoptively transferred to TNF-α–challenged WT or DREAM KO mice. 5 min later, intravital microscopy was performed. The number of rolling (H) and adherent (I) neutrophils. **(J–R)** Equal numbers of BM cells isolated from WT (CD45.1) and DREAM KO (CD45.2) were mixed and transplanted into irradiated WT (CD45.1) mice. **(J–M)** 6 wk after BM transplantation (BMT), blood was drawn. After RBC lysis, cells were labeled with isotype control IgGs, Alexa Fluor 488–conjugated anti-CD45.1, or PE-conjugated anti-CD45.2 antibodies. After gating a single neutrophil (J), the expression of CD45.1 and CD45.2 was evaluated in WT (K), DREAM KO (L), and BM chimeric mice (M) with flow cytometry. The representative data were obtained from three independent experiments. **(N–R)** BM chimeric mice were treated with intrascrotal injection of TNF-α and used for intravital microscopy. WT and KO neutrophils were visualized with Alexa Fluor 488–conjugated anti-CD45.1 and Alexa Fluor 647–conjugated anti-CD45.2 antibodies, respectively, along with PE-conjugated anti–Ly-6G antibodies. **(N)** Representative images. WT neutrophils: $CD45.1^+/Ly\text{-}6G^+$ (cyan) and DREAM KO neutrophils: $CD45.2^+/Ly\text{-}6G^+$ (purple). Large arrows: the direction of blood flow; small arrows: rolling neutrophils; arrowhead: adherent neutrophils. **(O)** The number of rolling neutrophils. **(P)** The cumulative frequency of the rolling velocity of neutrophils. **(Q and R)** The number of adherent and transmigrated neutrophils. The horizontal bar represents the median value in O and R. Otherwise, data represent the mean ± SD ($n$ = 41–48 venules in five mice/group). **(S–W)** Flow chamber assays were performed as described in the Materials and methods. **(S)** TNF-α–stimulated adherent WT and KO neutrophils. **(T)** Transmigrating TNF-α–stimulated WT neutrophils. **(U–W)** After a 10-min incubation with or without TNF-α or fMLP, the numbers of rolling, adherent, and transmigrated neutrophils were counted in a field of view (0.15 $mm^2$). Scale bars = 10 µm. Data represent the mean ± SD ($n$ = 4). The number of adherent neutrophils was counted in 4 additional areas ($n$ = 20 fields of view/group). *, P < 0.05; **, P < 0.01; ***, P < 0.001; ****, P < 0.0001 after ANOVA and either Tukey's test (B, D–I, and U–W) or Kruskal–Wallis test with post hoc Dunn's test (C), Mann–Whitney $U$ test (O, P, and R), and Student's $t$ test (Q). SSC-A, side scatter area; FSC-A, forward scatter area; FSC-H, forward scatter height.

mouse neutrophils and support that DREAM positively regulates the IKK–NF-κB signaling pathway.

### Neutrophil DREAM enhances the ligand-binding activity of β2 integrin through activated IKKβ

During vascular inflammation, αLβ2 integrin is required for slowing down rolling neutrophils and arresting them on activated ECs, whereas αMβ2 integrin mediates neutrophil crawling (Phillipson et al., 2006). Unlike other integrins, αMβ2 integrin is stored in secretory granules and translocates to the plasma membrane during neutrophil activation (Borregaard et al., 1994; Lominadze et al., 2005). Since neutrophil DREAM contributes to neutrophil recruitment during vascular inflammation, we assessed the expression level and activation state of neutrophil β2 integrins. Compared with WT neutrophils, DREAM KO neutrophils showed significantly lower surface amounts of αMβ2 integrin after stimulation with TNF-α but not fMLP (Fig. 4, A and B). We confirmed that the binding of soluble fibrinogen (Fg), a ligand for αMβ2 integrin, to TNF-α–stimulated neutrophils was impaired by DREAM deletion, whereas the ligand binding was not different when WT and KO neutrophils were stimulated with fMLP (Fig. 4 C). Similarly, DREAM deletion inhibited neutrophil adhesion to immobilized ICAM-1 after stimulation with TNF-α but not fMLP (Fig. 4 D). These results suggest that neutrophil DREAM plays an important role in TNF-α–induced β2 integrin activation.

Since neutrophil DREAM promotes neutrophil adhesive function (Fig. 2) and is important for TNF-α–induced IKK activation (Fig. 3 G), we sought to examine whether IKK regulates αMβ2 integrin function. Two structurally different IKK inhibitors, TPCA-1 (an IKKβ-selective inhibitor; Podolin et al., 2005) and Bay 11–7082 (an IKKα/β inhibitor; Rauert-Wunderlich et al., 2013), dose-dependently diminished IKK phosphorylation in TNF-α–stimulated neutrophils (Fig. 4, E and F). Furthermore, inhibition of IKKβ with TPCA-1 markedly blocked IκB degradation in TNF-α–stimulated neutrophils (Fig. 4 G). Treatment of WT neutrophils with TPCA-1 or Bay 11–7082 reduced the surface amount of αMβ2 integrin after stimulation with TNF-α but not fMLP, and neither inhibitor showed an additive effect in DREAM KO neutrophils (Fig. 4, H and I). The surface amount of αLβ2 integrin was similar in WT and DREAM KO neutrophils (Fig. 4 J). These results suggest that neutrophil DREAM promotes degranulation of αMβ2 integrin through TNF-α–activated IKKβ. We also examined the expression of other surface molecules essential for neutrophil rolling and tethering (Zarbock et al., 2011). The surface levels of PSGL-1, L-selectin, CD44, CXCR2, and CXCR4 were not affected by DREAM deletion (Fig. S3), suggesting that the increased rolling

Table 2. **The hemodynamic parameters in TNF-α–challenged DREAM BM chimeric mice**

| Mice | WBC (cells/µl) | % of neutrophils | Diameter of venules (µm) | Blood flow rate ($µl^{-6}/s$) |
|---|---|---|---|---|
| WT-BM → WT | 2,800 ± 660 | 37 ± 7 | 33.5 ± 4 | 456 ± 102 |
| WT-BM → KO | 3,400 ± 950 | 44 ± 8 | 35.1 ± 4 | 582 ± 129 |
| KO-BM → WT | 3,700 ± 1,120 | 45 ± 8 | 33.1 ± 3 | 605 ± 145 |
| KO-BM → KO | 3,600 ± 1,190 | 45 ± 9 | 36.2 ± 4 | 725 ± 153* |

All parameters were measured as described in Table 1. Data represent the mean ± SD ($n$ = 6 mice per group). *, P < 0.05 versus WT-BM → WT mice after ANOVA and Dunnett's test. WBC, white blood cells.

Table 3. **The number of circulating blood cells in WT, DREAM KO, and BM chimeric mice**

| | WBC ($10^3$/μl) | NE ($10^3$/μl) | LY ($10^3$/μl) | MO ($10^3$/μl) | RBC ($10^6$/μl) | PLT ($10^6$/μl) | MPV (fl) |
|---|---|---|---|---|---|---|---|
| WT (CD45.1) | 5.2 ± 2.7 | 0.8 ± 0.2 | 4.0 ± 1.5 | 0.2 ± 0.0 | 7.4 ± 1.7 | 882 ± 164 | 5.9 ± 0.9 |
| DREAM KO | 3.6 ± 0.8 | 0.7 ± 0.2 | 2.9 ± 1.3 | 0.1 ± 0.0 | 7.5 ± 1.4 | 976 ± 193 | 5.9 ± 1.0 |
| BM chimeric mice | 5.4 ± 1.7 | 0.9 ± 0.2 | 4.2 ± 1.7 | 0.3 ± 0.1 | 8.8 ± 1.0 | 1,215 ± 219 | 6.3 ± 1.0 |

The blood was obtained from 8–10-wk-old male WT (B6.SJL-*Ptprc*$^a$*Pepc*$^b$/BoyJ, a C57BL/6 congenic strain [CD45.1]) and DREAM KO mice and from BM chimeric mice at 6 wk after transplantation of an equal number of WT and KO BM cells into WT (CD45.1) mice. Blood cells were counted using HEMAVET 950 (Drew Scientific). Data represent the mean ± SD ($n$ = 6 mice per group). WBC, white blood cells; NE, neutrophils; LY, lymphocytes; MO, monocytes; PLT, platelets; MPV, mean platelet volume.

of DREAM KO neutrophils is likely to result from impaired β2 integrin function.

To investigate whether DREAM and IKK regulate β2 integrin activation, we used conformation-specific reporter antibodies against activated human β2 integrins. DREAM knockdown in dHL-60 cells abrogated the binding of antibodies against activated αMβ2 (CBRM1/5), extended αLβ2 (NKI-L16), or high-affinity β2 (mAb24), and significantly reduced the binding of antibodies against total αMβ2 (ICRF44) after TNF-α treatment (Fig. 4, K–N; Lefort et al., 2012; Li et al., 2014). These results suggest that DREAM positively regulates β2 integrin activation in TNF-α–stimulated dHL-60 cells. We also found that compared with vehicle control, TPCA-1 significantly inhibited the binding of the conformation-specific antibodies to TNF-α–stimulated human neutrophils (Fig. 4, O–R). This result suggests an important role of IKKβ in β2 integrin activation in human neutrophils.

The interaction between the cytoplasmic tail of the integrin β subunit and talin1 is the final step in integrin activation (Ye et al., 2011). Therefore, we investigated whether neutrophil DREAM and IKKβ affect the β2-talin1 interaction after agonist stimulation. Talin1 rapidly bound to β2 integrin after stimulation with fMLP or TNF-α (Fig. 4, S and T). Whereas β2-talin 1 binding disappeared 5 min after fMLP stimulation, the interaction persisted during 5 min after TNF-α stimulation, implying that activation of neutrophil β2 integrin has different kinetics after treatment with fMLP and TNF-α. We observed that β2-talin1 binding was enhanced in both WT and DREAM KO neutrophils 1 min after fMLP treatment (Fig. 4 U). In contrast, DREAM KO neutrophils treated with TNF-α for 2 min showed markedly lower β2-talin1 binding than WT neutrophils. In addition, treatment with TPCA-1 diminished β2-talin1 binding in TNF-α–stimulated neutrophils (Fig. 4 V). These results further support our conclusion that neutrophil DREAM and IKKβ augment β2 integrin activation after TNF-α stimulation.

Since $H_2O_2$ produced from neutrophil NADPH oxidase 2 is important for the activation and ligand-binding activity of αMβ2 integrin during neutrophil activation (Kim et al., 2015), we further examined whether DREAM affects the production of ROS. DREAM deletion significantly reduced ROS production from neutrophils adherent to immobilized Fg in the presence of TNF-α but not fMLP (Fig. S4). This result suggests the role of neutrophil DREAM in αMβ2 integrin function and then integrin outside-in signaling–induced ROS production after TNF-α stimulation.

### Neutrophil DREAM promotes degranulation through IKKβ–SNAP-23 signaling

Since neutrophil DREAM and IKKβ enhanced the surface amount of αMβ2 integrin after TNF-α stimulation, we determined whether neutrophil DREAM and IKKβ affect degranulation via exocytosis. As assessed by the activity of gelatinase (a marker for specific and gelatinase granules) in the releasate (Lominadze et al., 2005), loss of DREAM in mouse neutrophils and dHL-60 cells significantly inhibited enzyme activity in response to TNF-α but not fMLP (Fig. 5, A and B). Also, treatment with TPCA-1 or Bay 11–7082 diminished gelatinase activity in TNF-α–stimulated WT neutrophils (Fig. 5 C). However, when tested in DREAM KO neutrophils, TPCA-1 did not exhibit an additive effect. Pretreatment of human neutrophils with TPCA-1 reduced gelatinase activity in response to TNF-α but not fMLP (Fig. 5 D). These results suggest that neutrophil DREAM and IKKβ promote TNF-α–induced degranulation from specific and gelatinase granules in which αMβ2 integrin is localized (Lominadze et al., 2005). DREAM deletion did not alter azurophilic granule secretion induced by fMLP as assessed by myeloperoxidase (MPO) activity (Fig. 5 E). However, the inability of TNF-α to induce azurophilic granule secretion in neutrophils precluded evaluating the role of DREAM in azurophilic granule secretion.

Synaptosome-associated protein 23 (SNAP-23) phosphorylation is crucial for degranulation in activated mast cells (Hepp et al., 2005) and platelets (Karim et al., 2013). It is controversial whether IKKβ is responsible for SNAP-23 phosphorylation in activated platelets (Karim et al., 2013; Salzmann et al., 2020). We found that SNAP-23 was rapidly phosphorylated in TNF-α–stimulated WT neutrophils, and the phosphorylation was reduced in DREAM KO neutrophils (Fig. 5 F). Furthermore, pretreatment of neutrophils with TPCA-1 abrogated TNF-α–induced SNAP-23 phosphorylation (Fig. 5 G). Immunoprecipitation assays showed that the binding of SNAP-23 to phosphorylated IKK was enhanced in neutrophils 2–5 min after TNF-α stimulation (Fig. 5 H). These results suggest that DREAM positively regulates degranulation through IKKβ-phosphorylated SNAP-23 in TNF-α–stimulated neutrophils.

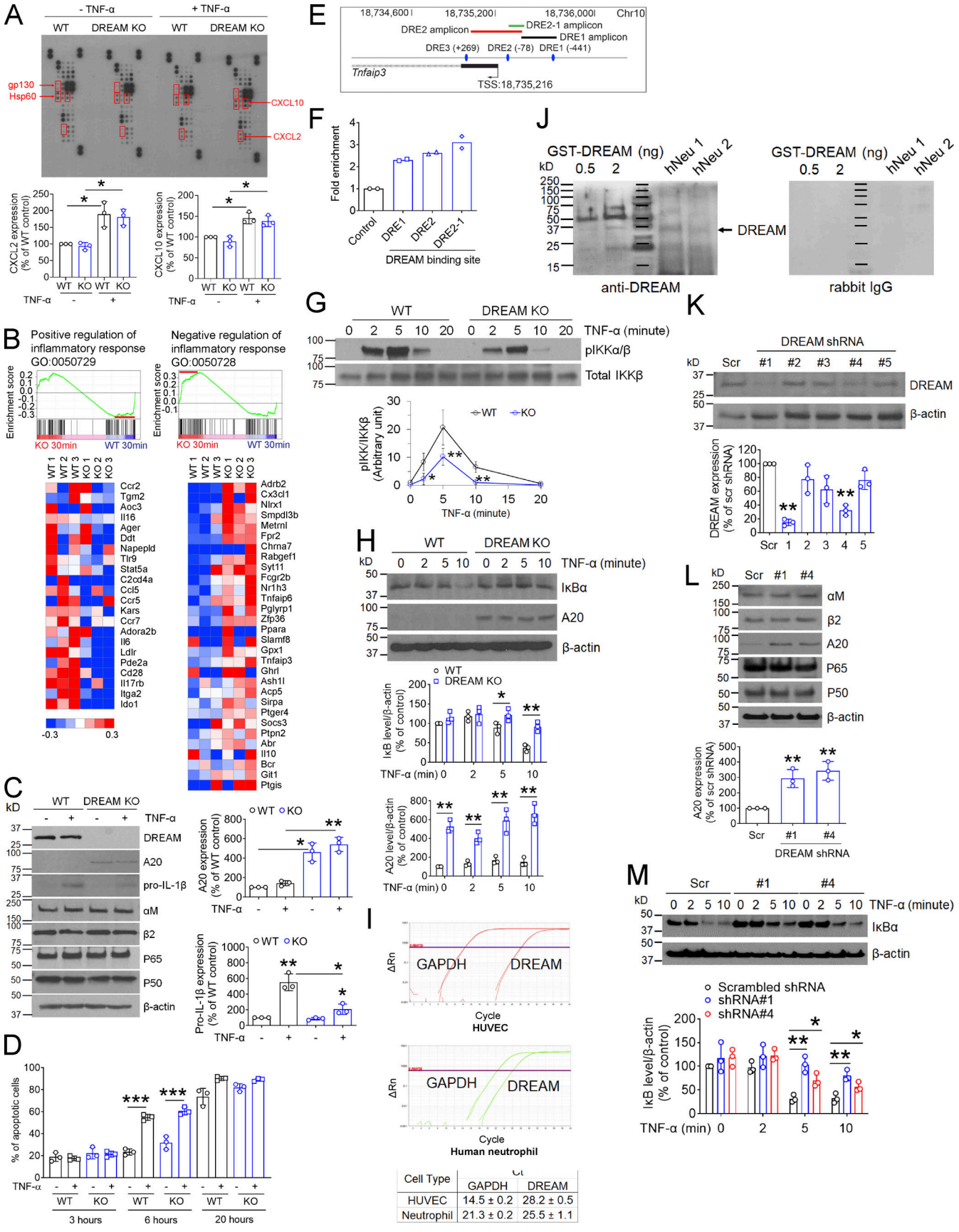


Figure 3. **Neutrophil DREAM down-regulates A20 expression and positively regulates NF-κB activity. (A)** Chemokine microarray with the lysate of WT and DREAM KO neutrophils treated without or with TNF-α for 3 h. HSP60 and gp130 were used as loading controls. Densitometric analysis of CXCL2 and

CXCL10 expression after normalization to HSP60 expression. **(B)** WT and DREAM KO neutrophils were treated with TNF-α for 30 min and subjected to RNA-seq. GSEA shows the gene expression altered by deletion of neutrophil DREAM. Heat map of genes selected from pro- and anti-inflammatory response pathways in WT and KO neutrophils ($n$ = 3). Red, up-regulation; blue, down-regulation. **(C)** WT and DREAM KO neutrophils were treated with or without 5 ng/ml TNF-α for 3 h. Equal amounts (50 µg) of proteins in cell lysates were immunoblotted. Representative blots ($n$ = 3). Densitometric analysis of A20 and pro–IL-1β expression. **(D)** WT and DREAM KO neutrophils were treated with 20 ng/ml TNF-α for 3, 6, and 20 h and used for flow cytometry with FITC-conjugated annexin V. **(E and F)** Mouse neutrophils were used for ChIP analysis. **(E)** The DREAM-binding sites (DRE sites) and transcriptional start sites (TSSs) in *Tnfaip3*. Three DRE amplicons using several different primers are shown. DRE1 amplicon: 18,735,396–18,735,671 (275 bp), DRE2 amplicon: 18,734,944–18,735,414 (469 bp), and DRE2-1 amplicon: 18,735,305–18,735,422 (117 bp). **(F)** DREAM enrichment was calculated by the fold increase in Gfi1b (control). Data represent the mean of two experiments. **(G)** WT and DREAM KO neutrophils were incubated with 5 ng/ml TNF-α for 0–20 min. Lysates were immunoblotted with antibodies against pIKKα/β or total IKKβ and subjected to densitometric analysis. **(H)** WT and DREAM KO neutrophils were incubated with 5 ng/ml TNF-α for 0–10 min and subjected to immunoblotting with antibodies against IκBα, A20, or β-actin, and densitometric analysis. **(I)** RT-qPCR of HUVECs and neutrophils. **(J)** GST-tagged DREAM (0.5 and 2 ng) expressed in *Escherichia coli* and lysates of neutrophils isolated from two donors (hNeu 1 and hNeu 2) were used for immunoblotting with rabbit anti-DREAM antibodies. Representative blots ($n$ = 3). **(K–L)** HL-60 cells treated with scrambled (Scr) or DREAM shRNAs were differentiated for 5–7 d and subjected to immunoblotting with the indicated antibodies and densitometric analysis. **(M)** dHL-60 cells were treated with 5 ng/ml TNF-α for 0–10 min and subjected to immunoblotting with anti-IκBα antibodies and densitometric analysis. Data represent the mean ± SD ($n$ = 3 or 4). *, P < 0.05; **, P < 0.01; and ***, P < 0.001 versus WT neutrophils or control shRNA after Student's $t$ test (D and G–M) or ANOVA and Tukey's test (C).

### Neutrophil DREAM promotes platelet–neutrophil aggregation under thromboinflammatory conditions

Platelets adhere to activated neutrophils on inflamed endothelium via the interactions of platelet P-selectin and glycoprotein Ibα with neutrophil PSGL-1 and activated αMβ2 integrin, respectively, forming microthrombi during vascular inflammation (Kim et al., 2015; Li et al., 2015; Li et al., 2019). Because neutrophil DREAM enhanced the ligand-binding activity of αMβ2 integrin, we sought to explore the effect of DREAM on platelet–neutrophil interactions. Under inflammatory conditions, platelets mainly attach to adherent neutrophils (Li et al., 2014; Li et al., 2019). Since deletion of neutrophil DREAM impaired neutrophil adhesion to TNF-α–inflamed endothelium (Fig. 2), we quantified platelet–neutrophil interactions by normalizing the fluorescence intensities of anti-CD42c antibodies to the number of adherent neutrophils. Intravital microscopy demonstrated that platelet–neutrophil interactions on the TNF-α–inflamed endothelium were significantly reduced in DREAM KO mice compared with WT mice (Fig. 6, A–C; Video 6; and Video 7). Furthermore, our studies using DREAM BM chimeric mice revealed that hematopoietic cell DREAM was responsible for platelet–neutrophil interactions in TNF-α–induced vascular inflammation (Fig. 6, D and E) and that nonhematopoietic cell DREAM did not appear to affect platelet–neutrophil interactions (P = 0.2529 at 120 s and P = 0.4618 at 180 s between WT-BM → WT and WT-BM → KO mice). These results suggest the role of both platelet and neutrophil DREAM in cell–cell aggregation.

Activated neutrophils and platelets promote heterotypic cell–cell aggregation under shear-mimicking conditions (Li et al., 2014; Li et al., 2019). Using flow cytometry, we observed that neutrophil–platelet aggregates were detected in the R1 gate (Fig. 6 F). Deletion of neutrophil DREAM significantly diminished platelet–neutrophil aggregation as assessed by the number of cell–cell aggregates and the fluorescence signal of anti-CD42c antibodies in the R1 gate (Fig. 6, G and H). Loss of platelet DREAM also perturbed platelet–neutrophil aggregation. Cell–cell aggregation was further inhibited when DREAM was deleted in both neutrophils and platelets. These results were confirmed by immunofluorescence microscopy in which the size of platelet–neutrophil aggregates was reduced by deletion of neutrophil or platelet DREAM (Fig. 6 I).

Pretreatment of human neutrophils or platelets with TPCA-1 significantly attenuated neutrophil–platelet aggregation (Fig. 6, J and K). This inhibitory effect was potentiated when both neutrophils and platelets were treated with the inhibitor. Although the contribution of IKKβ to granule secretion from activated platelets is controversial (Karim et al., 2013; Salzmann et al., 2020), we found that pretreatment with TPCA-1 significantly inhibited P-selectin exposure in thrombin-activated human platelets (Fig. 6 L). In addition, we confirmed that compared with WT platelets, DREAM-null platelets exhibited significantly lower P-selectin exposure in response to a low concentration of thrombin, as we reported previously (Kim et al., 2017b; Fig. 6 M). Deletion of platelet DREAM diminished the interaction with WT neutrophils, and pretreatment of DREAM KO platelets with anti–P-selectin antibodies did not show an additive effect on the platelet–neutrophil interaction (Fig. 6 N). Overall, since neutrophil αMβ2 integrin and PSGL-1 interact with platelet glycoprotein Ibα and P-selectin, respectively (Konstantopoulos et al., 1998; Li et al., 2015), these results suggest that DREAM and IKKβ enhance neutrophil αMβ2 function and platelet P-selectin exposure, contributing to platelet–neutrophil aggregation under thromboinflammatory conditions.

### DREAM enhances interactions of neutrophils with ECs and platelets in microvessels of SCD mice under severe inflammatory conditions

SCD is characterized by RBC hemolysis, chronic inflammation, and organ damage (Zhang et al., 2016). Recurrent vaso-occlusive pain crisis, the hallmark of SCD, is mediated by intravascular cell–cell aggregation. Since our data demonstrated a crucial role of neutrophil DREAM in neutrophil–EC and neutrophil–platelet interactions, we explored whether DREAM affects vaso-occlusive events in SCD. We first generated SCD ($Hbb^{-/-}$) mice deficient in DREAM in nonhematopoietic and/or hematopoietic cells (Fig. 6 O). The chimeric mice expressed the human HbS transgene as we described previously (Fig. S5, A and B; Kim et al., 2017a). Compared with WT mice, all chimeric SCD mice had leukocytosis and anemia (Table 4). SCD mice with DREAM deficiency in nonhematopoietic cells, compared with other groups, resulted in a significant increase in the numbers of

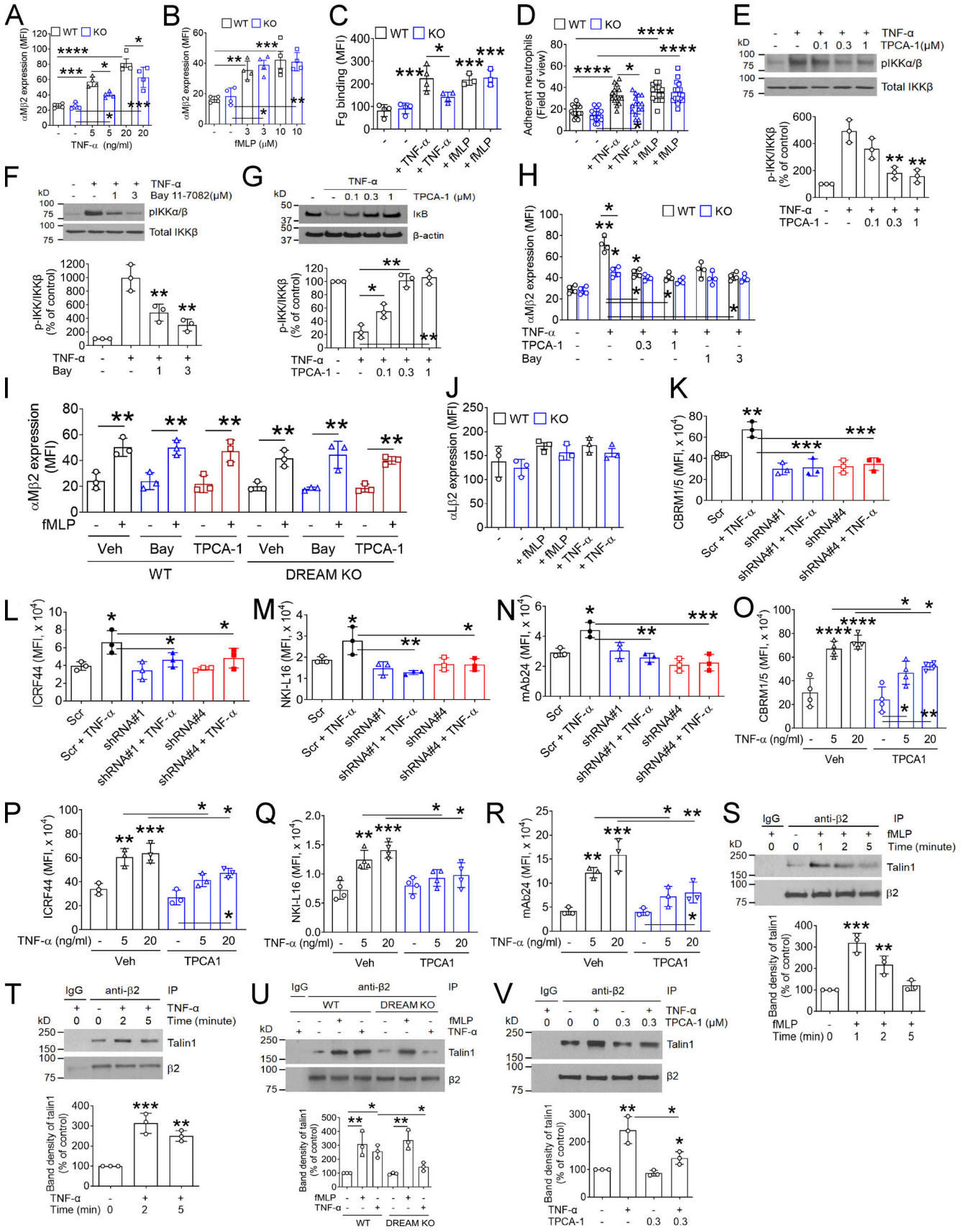

Figure 4. **Neutrophil DREAM enhances the ligand-binding function of β2 integrin through activated IKKβ. (A–C)** WT and DREAM KO neutrophils were treated with or without 5 ng/ml TNF-α or 10 µM fMLP for 10 min unless otherwise stated. Flow cytometry was performed with anti-αMβ2 or anti-αLβ2

antibodies, and DyLight 488–conjugated Fg. **(D)** WT and DREAM KO neutrophils were placed on immobilized ICAM-1 in the presence or absence of TNF-α or fMLP. Adherent cells were counted under a microscope. **(E–J)** WT and DREAM KO neutrophils were pretreated with or without 0.1% DMSO (– or vehicle [Veh]), TPCA-1 (an IKKβ-selective inhibitor, 0.1–1 μM), or Bay 11–7082 (Bay; an IKKα/β inhibitor, 1–3 μM) and then incubated with or without TNF-α or fMLP for (E–G) 5 or (H–J) 10 min. **(E–G)** Lysates were immunoblotted with antibodies against pIKKα/β or total IKKβ and subjected to densitometric analysis (mean ± SD, $n = 3$). **(H–J)** Flow cytometry was performed with anti-αMβ2 or anti-αLβ2 antibodies. **(I)** TPCA-1: 0.3 μM and Bay: 3 μM. **(K–N)** dHL-60 cells were treated with or without TNF-α for 10 min and subjected to flow cytometry with antibodies against activated αMβ2 (CBRM1/5), total αMβ2 (ICRF44), extended αLβ2 (NKI-L16), or activated β2 (mAb24). **(O–R)** Human neutrophils were pretreated with 0.1% DMSO (Veh) or 0.3 μM TPCA-1, stimulated with TNF-α, and used for flow cytometry. The MFI values were measured. **(S and T)** WT neutrophils were treated with or without fMLP or TNF-α for 0–5 min. Lysates were immunoprecipitated with control IgG or anti-β2 antibodies and subjected to immunoblotting with antibodies against talin1 or β2 and densitometric analysis. **(U and V)** WT or DREAM KO neutrophils were pretreated with or without vehicle or TPCA-1 and stimulated with fMLP or TNF-α. Talin1-β2 binding was detected as described above. Data represent the mean ± SD ($n = 3$ or 4). *, $P < 0.05$; **, $P < 0.01$; ***, $P < 0.001$; ****, $P < 0.0001$ after ANOVA and either Dunnett's test (E–G, versus vehicle control [+ TNF-α], and S and T, versus unstimulated control [–]) or Tukey's test. IP, immunoprecipitation; Scr, scrambled.

leukocytes, lymphocytes, and RBCs without affecting those of neutrophils and monocytes (Table 4; and Fig. S5, C–G). The number of platelets in SCD mice was decreased by DREAM deficiency in nonhematopoietic or hematopoietic cells, or both, yet remained in a normal range (Fig. S5 H).

Intravital microscopy revealed that deficiency in either nonhematopoietic or hematopoietic DREAM significantly reduced the number of adherent neutrophils to ECs without affecting the number of rolling neutrophils in TNF-α–challenged SCD mice (Fig. 6, P and Q). Non-hematopoietic and hematopoietic DREAM-deficient SCD mice, compared with either nonhematopoietic or hematopoietic DREAM-deficient SCD mice, did not show an additive effect on neutrophil–EC interactions, implying that hematopoietic and nonhematopoietic DREAM are likely to induce neutrophil–EC interactions by enhancing the association between neutrophil β2 integrin and EC ICAM-1. Loss of either nonhematopoietic or hematopoietic DREAM inhibited platelet–neutrophil interactions (Fig. 6 R) and appeared to increase the blood flow rates (Fig. 6 S). Several studies have shown that TNF-α challenge and surgical procedures cause death in SCD mice due to severe inflammatory conditions and vaso-occlusive events (Barazia et al., 2015; Jang et al., 2012). We found that SCD mice with hematopoietic DREAM deficiency significantly improved the survival of TNF-α–challenged SCD mice (Fig. 6 T), whereas SCD mice with nonhematopoietic DREAM deficiency exhibited marginal improvement in survival. However, since no noticeable organ damage was observed in SCD mice (data not shown), a result likely to be explained by their relatively young age (3–4 mo after BM transplantation; Li et al., 2020; Nasimuzzaman et al., 2019), we were unable to evaluate the effect of DREAM deletion on organ damage. Overall, our results provide evidence that deletion of DREAM inhibits intravascular cell–cell interactions and vaso-occlusive events in TNF-α–challenged SCD mice. It would be of interest to test the long-term effect of DREAM deficiency on organ damage in SCD mice.

To further confirm the role of neutrophil DREAM in neutrophil recruitment on inflamed microvessels of SCD mice, we labeled WT and DREAM KO neutrophils with different dyes and injected an equal number of WT and KO cells into TNF-α–challenged SCD mice. Compared with WT neutrophils, DREAM KO neutrophils exhibited significantly increased rolling and decreased adhesion on the inflamed venular endothelium (Fig. 6, U–W). Therefore, as seen in TNF-α–challenged WT mice (Fig. 2), neutrophil DREAM is likely to promote neutrophil recruitment to sites of inflammation in SCD.

## Discussion

In the present study, we discovered that neutrophil DREAM positively regulates neutrophil adhesive function during TNF-α–induced vascular inflammation. As seen in ECs (Tiruppathi et al., 2014), neutrophil DREAM represses A20 expression and promotes IKKβ–NF-κB signaling. Furthermore, neutrophil DREAM promotes IKKβ-mediated β2 integrin activation and degranulation after TNF-α stimulation. Importantly, our in vivo studies in SCD mice provide evidence that targeting DREAM may be a therapeutic strategy to attenuate intravascular cell–cell interactions and vaso-occlusive events in SCD.

The binding of TNF-α to its receptor recruits many molecules, such as TRAFs and RIPKs (Cabal-Hierro and Lazo, 2012), and induces IKK activation and NF-κB–mediated transcription of pro-inflammatory genes, including cytokines (e.g., TNF-α and ILs) and cell adhesion molecules (e.g., ICAM-1 and E-selectin; http://www.bu.edu/nf-kb/gene-resources/target-genes/; Zhang et al., 2017). We found that deficiency in nonhematopoietic DREAM inhibits the expression of ICAM-1 but not E-/P-selectins on the TNF-α–inflamed endothelium. Despite no significant difference in chemokine production between WT and DREAM KO neutrophils, deletion of neutrophil DREAM down-regulated the expression of genes associated with inflammatory responses and impaired IKKβ activation after TNF-α stimulation. p50 and p52 induce gene transcription by forming heterodimers with other NF-κB family proteins, such as p65, RelB, or c-Rel, or by recruiting proteins containing C-terminal transcription activation domains (Hayden and Ghosh, 2011). However, when p50 and p52 bind to DNA as homodimers, they cannot induce gene transcription but rather repress transcription (Hayden and Ghosh, 2011). Unlike ECs and lymphocytes, neutrophils do not express p52 (McDonald et al., 1997). These findings suggest that the NF-κB complex may form different dimers and distinctly regulate gene transcription in different cell types. We found that neutrophil DREAM, like EC DREAM (Tiruppathi et al., 2014), represses A20 expression through direct binding to DRE sites in the promoter region of *Tnfaip3* and promotes NF-κB activity. Previous studies have demonstrated that A20 possesses both deubiquitinase and ubiquitin E3 ligase activities, which are required to terminate NF-κB activity (Boone et al., 2004; Wertz

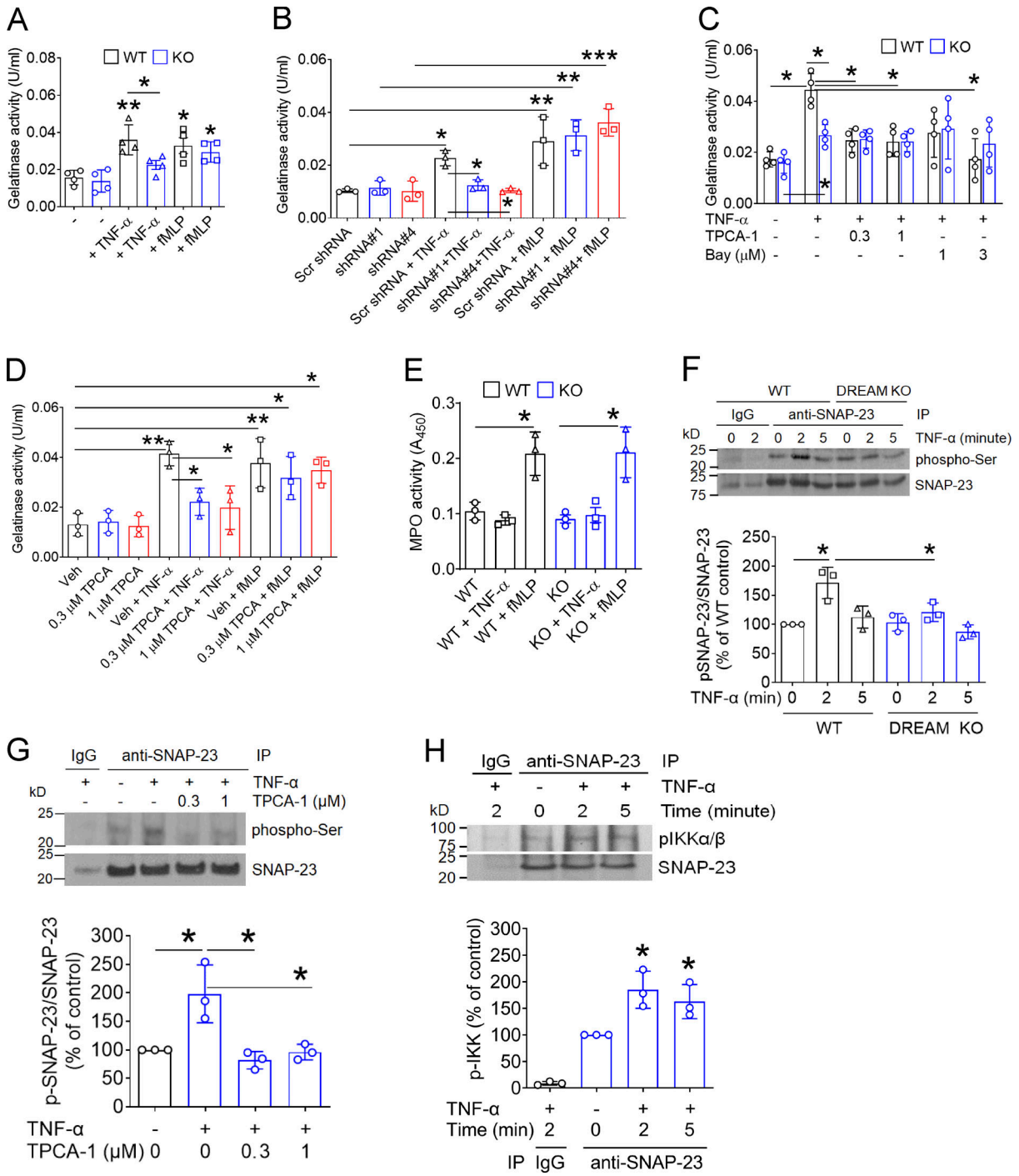


Figure 5. **Neutrophil DREAM promotes degranulation through IKKβ-mediated SNAP-23 phosphorylation. (A and C)** WT and DREAM KO neutrophils were treated without (A) or with (C) vehicle (–, 0.1% DMSO) or a different concentration of TPCA-1 and Bay 11–7082. Cells were then incubated with 5 ng/ml TNF-α or 10 μM fMLP for 10 min. The releasate was used to measure gelatinase activity ($n$ = 3). **(B)** dHL-60 cells pretreated with control or DREAM shRNA were incubated with TNF-α or fMLP. The supernatant was collected and used in the gelatinase activity assay. **(D)** Human neutrophils were pretreated with 0.3–1 μM TPCA-1 and then incubated with or without TNF-α or fMLP. The supernatant was collected and used in the gelatinase activity assay. **(E)** WT and DREAM KO neutrophils were treated with or without TNF-α or fMLP and used for an MPO activity assay with the supernatant. **(F)** WT or DREAM KO neutrophils were treated with or without TNF-α for 0–5 min. **(G)** WT neutrophils were pretreated with 0.1% DMSO (–) or 0.3–1 μM TPCA-1 and then treated with or without TNF-α for 5 min. **(H)** WT neutrophils were treated with or without TNF-α for 2 or 5 min. The lysates were immunoprecipitated with control IgG or anti–SNAP-23 antibodies and subjected to immunoblotting with anti–phospho-Ser, anti–SNAP-23, or anti-pIKKα/β antibodies and densitometric analysis. Data represent the mean ± SD ($n$ = 3 or 4). *, P < 0.05; **, P < 0.01; ***, P < 0.001 versus unstimulated neutrophils or two groups after Student's $t$ test (A and E) or after ANOVA and either Tukey's test (B–D, F, and G) or Dunnett's test (H). Bay, Bay 11–7082; IP, immunoprecipitation; Scr, scrambled; Veh, vehicle.

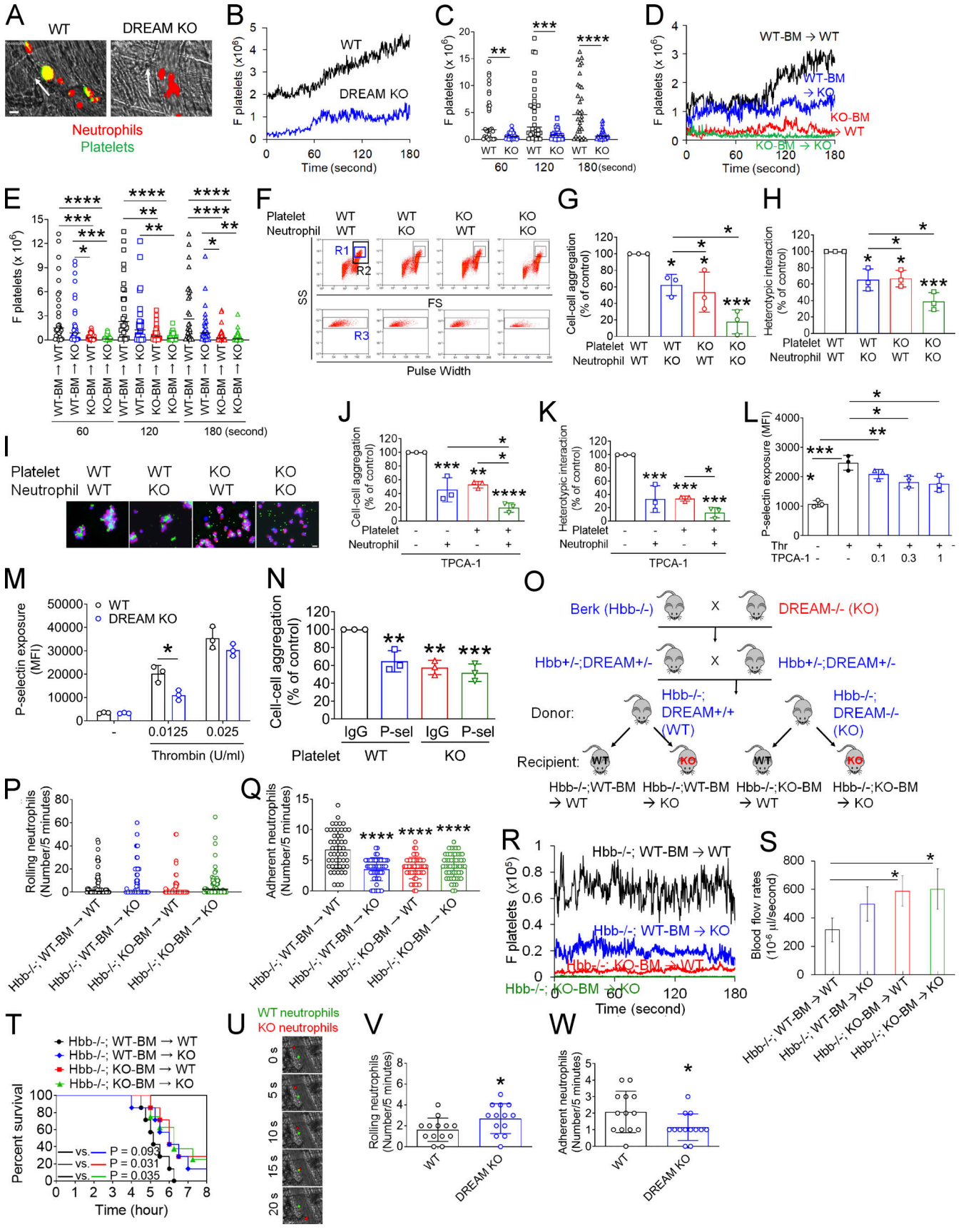


Figure 6. **DREAM positively regulates platelet–neutrophil aggregation and vaso-occlusive events under thromboinflammatory conditions. (A–E)** Intravital microscopy on WT, DREAM KO, or BM chimeric mice was performed as described in Fig. 1. Neutrophils and platelets on inflamed venules were

visualized with Alexa Fluor 647–conjugated anti–Ly-6G and Dylight 488–conjugated anti-CD42c antibodies, respectively. **(A)** Representative images. **(B and D)** The integrated median fluorescence intensity values of the anti-CD42c antibody (F platelets) were normalized to the number of adherent neutrophils and the length of vessels and plotted as a function of time. **(C and E)** F platelets were compared at 60, 120, and 180 s. The horizontal bar represents the median value ($n$ = 30–32 venules in four mice/group). **(F–I)** In vitro platelet–neutrophil aggregation was conducted under stirring conditions as described in the Materials and methods. **(F)** R1, platelet–neutrophil aggregates; R2, neutrophils; and R3, the number of cell aggregates in the R1 gate. Neutrophil–platelet aggregation was quantified by (G) the number of cell–cell aggregates and (H) the fluorescence signal of anti-CD42c antibodies in the R1 gate (heterotypic interaction). **(I)** Antibody-labeled neutrophils and platelets were mixed under stirring conditions. After cytospin, fluorescence microscopy was performed. Neutrophils: red; platelets: green; DAPI: blue. Representative images ($n$ = 3). **(J and K)** Human neutrophils and platelets were pretreated with or without 0.3 µM TPCA-1. After labeling with FITC-conjugated anti–L-selectin or APC-conjugated anti-CD41 antibodies, neutrophils and platelets were treated with TNF-α and thrombin, respectively. Cells were mixed, and neutrophil–platelet aggregates were quantified as described above. **(L)** Human platelets were pretreated with vehicle (–) or 0.1–1 µM TPCA-1 and then with thrombin (Thr). **(M)** P-selectin exposure was measured in resting and thrombin-activated WT and DREAM KO platelets by flow cytometry. **(N)** Platelet–neutrophil aggregation was performed as described above. Platelets were treated with thrombin in the presence of control IgG or anti–P-selectin antibodies, incubated with activated WT neutrophils, and then subjected to flow cytometry. Data represent the mean ± SD ($n$ = 3). **(O–W)** SCD mice deficient in nonhematopoietic and/or hematopoietic DREAM were treated with i.p. injection of TNF-α. Intravital microscopy was conducted as described above. **(O)** Generation of nonhematopoietic and/or hematopoietic DREAM-deficient SCD mice. **(P and Q)** The number of rolling and adherent neutrophils. **(R)** Adherent/aggregating platelets were quantified by the integrated fluorescence intensity value of the anti-CD42c antibody (F platelets). **(S)** Fluorescently labeled microspheres were injected into all mice, and the centerline velocity was calculated to assess blood flow rates. The horizontal bar represents the median value ($n$ = 20 vessels in four mice/group). Otherwise, data represent the mean ± SD ($n$ = 46–50 [for Q] or 12 venules [for S] in eight mice/group). **(T)** Survival curves during or after intravital microscopy. **(U–W)** Equal numbers of calcein-AM–labeled WT and CellTracker Deep Red–labeled DREAM KO neutrophils were injected into TNF-α–challenged SCD mice. Intravital microscopy was performed as described in Fig. 1. **(U)** Representative images. **(V and W)** The number of rolling and adherent neutrophils. Scale bars = 10 µm (A, I, and U). *, P < 0.05; **, P < 0.01; ***, P < 0.001; ****, P < 0.0001 after Mann–Whitney $U$ test (C), Student's $t$ test (M, V, and W), ANOVA and either Kruskal–Wallis test with post hoc Dunn's test (E) or Tukey's test (G, H, J–L, N, Q, and S), and Mantel–Cox log-rank test (T). P-sel, P-selectin; SS, side scatter; FS, forward scatter; Berk, Berkeley mice.

et al., 2004), and that A20 is crucial for LPS-induced NF-κB activity in macrophages and modifies ubiquitination on TRAF6 and RIPKs (Boone et al., 2004; Wertz et al., 2004). Another study has shown that A20 deletion in myeloid cells protects mice against influenza A virus–induced lung injury associated with increased influx of neutrophils and increased numbers of alveolar macrophages, which enhances viral clearance (Maelfait et al., 2012). Nevertheless, the molecular mechanism by which neutrophil DREAM-A20 signaling modulates TNF-α–induced signaling, including IKKβ activation, in vascular inflammation remains to be determined.

Capture or tethering of circulating neutrophils on inflamed endothelium results from the interactions between EC E-/P-selectins and neutrophil counter-receptors (e.g., PSGL-1, ESL-1, and CD44) and between chemokines on the EC surface and neutrophil receptors (e.g., CXCR2 and CXCR4), leading to integrin activation (Phillipson and Kubes, 2011). Subsequently, the binding of activated αLβ2 and αMβ2 integrins to ICAM-1 mediates slow rolling, arrest, adhesion, and crawling of neutrophils on inflamed endothelium. An in vitro study has shown that short-term treatment with TNF-α promotes neutrophil migration by up-regulating αMβ2 integrin (Montecucco et al., 2008). Using a flow chamber assay, we found that a 10-min incubation with TNF-α significantly enhances neutrophil adhesion to the stimulated EC monolayer and that neutrophil DREAM positively regulates neutrophil recruitment induced by TNF-α but not fMLP (Fig. 2, U–W). These results suggest that neutrophil DREAM promotes neutrophil adhesive function via an NF-κB–independent mechanism after TNF-α stimulation. Furthermore, our studies demonstrated that neutrophil DREAM and IKKβ augment activation of αMβ2 and αLβ2 integrins after short-term treatment with TNF-α but not fMLP (Fig. 4). Although initial injection of TNF-α into mice induces neutrophil recruitment by up-regulation of the expression of EC adhesion molecules, TNF-α produced from inflamed cells is likely to facilitate activation of neutrophil β2 integrin, contributing to neutrophil recruitment during vascular inflammation. Furthermore, we found that deletion of neutrophil DREAM does not affect the expression of neutrophil rolling and chemokine receptors and that neutrophil DREAM increases inside-out signaling of β2 integrin through TNF-α–activated IKKβ. These results suggest that the increased rolling number and speed of

Table 4. **The number of circulating blood cells in SCD mice deficient in non-hematopoietic and/or hematopoietic DREAM**

| Mice | WBC ($10^3$/µl) | NE ($10^3$/µl) | LY ($10^3$/µl) | MO ($10^3$/µl) | RBC ($10^6$/µl) | PLT ($10^3$/µl) | MPV (fl) |
|---|---|---|---|---|---|---|---|
| WT (C57BL/6J) | 4.0 ± 0.9 | 0.7 ± 0.2 | 3.1 ± 0.9 | 0.1 ± 0.0 | 10.5 ± 1.2 | 1,302 ± 302 | 7.0 ± 0.6 |
| $Hbb^{-/-}$; WT-BM → WT | 25.1 ± 6.7 | 2.5 ± 1.2 | 20.6 ± 5.5 | 1.9 ± 0.5 | 4.6 ± 0.4 | 1,760 ± 328.2 | 5.1 ± 0.2 |
| $Hbb^{-/-}$; WT-BM → KO | 41.5 ± 5.8** | 1.6 ± 0.5 | 39.4 ± 5.1*** | 2.8 ± 0.6 | 5.7 ± 0.6* | 1,175 ± 121.3*** | 4.8 ± 0.2 |
| $Hbb^{-/-}$; KO-BM → WT | 28.1 ± 10.1 | 2.2 ± 0.8 | 23.5 ± 8.2 | 2.3 ± 1.3 | 5.0 ± 0.5 | 1,271 ± 199.5** | 5.0 ± 0.1 |
| $Hbb^{-/-}$; KO-BM → KO | 34.6 ± 3.2 | 2.3 ± 0.5 | 29.7 ± 2.6 | 2.6 ± 0.4 | 4.5 ± 0.5 | 1,429 ± 117.3* | 5.2 ± 0.2 |

Blood cells from mice were counted using HEMAVET 950 (Drew Scientific). Data represent the mean ± SD ($n$ = 6 mice per group). WT (C57BL/6J) male mice were 8 wk old. *, P < 0.05; **, P < 0.01; ***, P < 0.001 versus $Hbb^{-/-}$ after ANOVA and Dunnett's test (four $Hbb^{-/-}$ chimeric groups). WBC, white blood cells; NE, neutrophils; LY, lymphocytes; MO, monocytes; PLT, platelets; MPV, mean platelet volume.

neutrophils in DREAM KO mice are likely to result from the impairment of αLβ2 integrin function.

Neutrophils have several secretory granules containing antimicrobial proteins, proteases, components of the respiratory burst oxidase, and membrane-bound receptors (Lominadze et al., 2005). We observed that neutrophil DREAM-enhanced IKKβ activation promotes degranulation from specific and gelatinase granules in TNF-α–stimulated neutrophils. Degranulation is controlled by the interactions between the vesicle and target membrane–specific soluble N-ethylmaleimide sensitive factor attachment protein receptor proteins (v- and t-SNAREs; Logan et al., 2003). It was reported that SNAP-23 is primarily detected in the specific and gelatinase granules and translocates to the plasma membrane during neutrophil activation (Martín-Martín et al., 2000). In platelets, IKKβ phosphorylates Ser95 in SNAP-23, which is critical for granule secretion following agonist stimulation (Karim et al., 2013). Since deletion of DREAM or inhibition of IKKβ impairs SNAP-23 phosphorylation and degranulation in TNF-α–stimulated neutrophils, our results suggest that neutrophil DREAM promotes degranulation through IKKβ-phosphorylated SNAP-23.

Blocking excessive neutrophil recruitment has beneficial effects on vascular inflammation (Gómez-Moreno et al., 2018), ischemia-reperfusion injury (Kim et al., 2015), and SC-induced vaso-occlusion (Barazia et al., 2015; Chang et al., 2010). TNF-α challenge of SCD mice causes severe inflammation in which most neutrophils adhere to the vessel wall and support adhesion and aggregation of other blood cells, thereby resulting in acute vaso-occlusion (Barazia et al., 2015; Li et al., 2019; Turhan et al., 2002). To reduce the frequency of vaso-occlusive pain crises in patients with SCD, the Food and Drug Administration has approved crizanlizumab, a humanized anti–P-selectin antibody that blocks leukocyte–EC interactions. We found that deficiency in nonhematopoietic or hematopoietic DREAM in SCD mice significantly diminishes neutrophil–EC interactions in microvessels after TNF-α challenge. Importantly, DREAM deficiency in hematopoietic or both hematopoietic/nonhematopoietic cells increases the blood flow rates and improves the survival of TNF-α–challenged SCD mice. Overall, these results indicate that DREAM promotes intravascular cell–cell interactions and vaso-occlusive events in SCD mice. A limitation of our study is that we were unable to determine the contribution of neutrophil DREAM to vaso-occlusive events in SCD mice since technical difficulties prevented us from generating neutrophil DREAM-deficient SCD mice.

Given that the numbers of circulating blood cells do not significantly differ between WT and DREAM KO mice and their BM chimeric mice (Table S1 and Table S2; Kim et al., 2017b), how nonhematopoietic DREAM deficiency in SCD mice increases the number of circulating lymphocytes and RBCs remains puzzling. Together with hematopoiesis, the timely mobilization of hematopoietic stem and progenitor cells from the BM into circulation is crucial for maintaining blood cell homeostasis (Mazo et al., 2011). Further investigation is required to determine the mechanism by which nonhematopoietic DREAM regulates the number of lymphocytes and RBCs in SCD. Cheng et al. (2002) reported that DREAM deletion in mice markedly attenuates pain responses by enhancing prodynorphin expression in the spinal cord. Although modulation of blood flow and vaso-occlusive events in SCD mice may not correlate with alleviation of inflammatory and neuropathic pain in patients, our results provide evidence that DREAM may be a novel therapeutic target to reduce intravascular cell–cell aggregation and vascular occlusive pain crises in SCD.

## Materials and methods

### Reagents

fMLP, human thrombin, puromycin, polybrene, 3, 3′, 5, 5′-tetramethylbenzidine liquid substrate, human KCNIP3 (DREAM) shRNAs (TRCN0000017600 [shRNA#1], TRCN0000017598 [shRNA#2], TRCN0000442186 [shRNA#3], TRCN0000017602 [shRNA#4], and TRCN0000017601 [shRNA#5]), scramble shRNA, and rabbit polyclonal anti-DREAM antibodies were purchased from Sigma-Aldrich. TPCA-1, a selective inhibitor of IKKβ (Podolin et al., 2005), and Bay 11–7082, an inhibitor of both IKKα and IKKβ (Rauert-Wunderlich et al., 2013), were from Cayman Chemical. Recombinant murine and human TNF-α, isotype control IgGs, PE- or Alexa Fluor 647–conjugated anti-mouse Ly-6G (1A8), APC-conjugated anti-mouse PECAM-1 (MEC13.3), anti-mouse ICAM-1 (YN1/1.7.4), PE-conjugated anti-mouse αM (M1/70), PE-conjugated anti-mouse CD11a (M17/4), PE-conjugated anti-mouse PSGL-1, PE-conjugated anti-human αMβ2 (ICRF44), PE-conjugated anti-mouse CXCR4 (L276F12), PE–anti-activated human αMβ2 (CBRM1/5), FITC-conjugated anti-human L-selectin (DREG-56), Alexa Fluor 488–conjugated anti-mouse/human CD44 (IM7), Alexa Fluor 647–conjugated anti-mouse CXCR2 (SA045E1), FITC-conjugated anti-mouse L-selectin (MEL-14), anti-mouse/rat P-selectin (RMP-1), PE- or Alexa Fluor 647–conjugated anti-mouse CD45.2 (QA18A15 and 104), Alexa Fluor 488–conjugated anti-mouse CD45.1 (A20), and anti-mouse/rat E-selectin antibodies (RME-1/CD62E) were purchased from BioLegend. Antibodies against DREAM, p50, A20, αM, β2, talin-1, or SNAP-23 and protein A/G agarose beads were obtained from Santa Cruz Biotechnology. DyLight 488–conjugated anti-mouse CD42c antibodies were from Emfret Analytics. Monoclonal antibodies against phosphoIKKα-Ser176/180 and phosphoIKKβ-Ser177/Ser181 (pIKKα/β), IKKβ, phosphoSer, IκBα, or p65 were obtained from Cell Signaling Technology. D-Phe-Pro-Arg-chloromethylketone was purchased from EMD Millipore. Polyclonal anti-actin antibodies were from Novus Biologicals. Goat polyclonal anti-human β2 and anti–IL-1β antibodies, recombinant mouse ICAM-1, and a mouse chemokine array kit were purchased from R&D Systems. DyLight 488–conjugated goat anti-rat IgG and anti-mouse IgG antibodies, Tissue-Plus OCT compound, Lipofectamine 2000 transfection reagent, and EnzChek Gelatinase/Collagenase Assay kit were from Thermo Fisher Scientific. Blocking anti-mouse P-selectin (RB40.34), APC-conjugated anti-human CD41a (HIP8), and PE-conjugated anti-human P-selectin (AK-4) antibodies were obtained from BD Bioscience. A monoclonal anti-activated human β2 antibody (mAb24) was obtained from Hycult Biotech. A monoclonal anti-activated human αLβ2 antibody (NKI-L16) was purchased from OriGene. Vectashield Antifade mounting medium containing DAPI was obtained from Vector Laboratories. Purified human Fg was kindly

provided by Deane F. Mosher (University of Wisconsin–Madison, Madison, WI; Cho et al., 2005). Fg was conjugated with DyLight 488 according to the manufacturer's instructions.

### Mice

WT (C57BL/6J, 6–8 wk old), B6.SJL-*Ptprc*$^{a}$*Pepc*$^{b}$/BoyJ (C57BL/6 congenic strain [CD45.1], 6–8 wk old), and Berkeley (SCD) (Tg [Hu-miniLCRα1 $^{G}\gamma^{A}\gamma\delta\beta^{S}$] *Hba*$^{-/-}$*Hbb*$^{-/-}$) mice were obtained from The Jackson Laboratory. DREAM KO mice were kindly provided by Josef Penninger (University of British Columbia, Vancouver, Canada; Cheng et al., 2002) and backcrossed for 10 generations on the background of C57BL/6J mice. Age-matched male and female WT and DREAM KO mice were used in all studies except intravital microscopy, in which age-matched male mice were used.

To generate DREAM BM chimeric mice, BM cells from WT or DREAM KO mice were transplanted into lethally irradiated WT or DREAM KO mice. Furthermore, we generated BM chimeric mice with both WT and DREAM KO hematopoietic cells. BM cells isolated from congenic WT (CD45.1) and DREAM KO (CD45.2) mice were mixed with an equal number ($2 \times 10^6$ each) and transplanted into lethally irradiated WT (CD45.1) mice. 6–8 wk after transplantation, the chimeric mice were used for intravital microscopy. To generate DREAM KO SCD mice, DREAM male KO mice were bred with Hbb$^{+/-}$ female mice. Hbb$^{+/-}$;DREAM$^{+/-}$ mice were bred with each other to obtain Hbb$^{-/-}$;DREAM$^{+/+}$ (SCD) and Hbb$^{-/-}$;DREAM$^{-/-}$ (DREAM-deficient SCD) mice. Chimeric SCD mice were generated by transplantation of BM cells isolated from SCD or DREAM-deficient SCD mice into lethally irradiated male WT or DREAM KO mice (Li et al., 2020). 3 mo after transplantation, PCR analysis verified that chimeric mice expressed the transgene (human HbS) as we described previously (Kim et al., 2017a). DREAM KO mice were genotyped with tail biopsies and blood by Transnetyx. The following probes were used for RT-qPCR: *Kcnip3-1* WT forward primer, 5′-CAG ACAGCAGTGACAGTGAACT-3′, reverse primer, 5′-GGTGAACTT GGTCTGAGCTTGTAG-3′, and reporter, 5′-CTGGCTGATGGCGCA CC-3′; and neomycin forward primer, 5′-GGGCGCCCGGTTCTT-3′, reverse primer, 5′-CCTCGTCCTGCAGTTCATTCA-3′, and reporter, 5′-ACCTGTCCGGTGCCC-3′. The chimeric SCD mice were used at the age of 24–28 wk. All animal care and experimental procedures were approved by the Institutional Animal Care and Use Committee at the University of Illinois at Chicago and Washington University School of Medicine.

### Isolation of neutrophils and platelets

For mouse neutrophils, BM cells were obtained from the femur and tibia of WT and DREAM KO mice by flushing with HBSS containing 20 mM Hepes, pH 7.4, and 0.1% BSA. The cell suspension was filtered through 40-μM nylon meshes and centrifuged at 300 *g* at 4°C for 10 min. After resuspension with HBSS, cells were laid on the top of 63% Percoll solution and centrifuged at 1,200 *g* at 4°C for 30 min. After RBCs were lysed using a lysis buffer (Sigma-Aldrich), neutrophils were centrifuged at 800 *g* at 4°C for 5 min and resuspended with HBSS containing 1 mM $MgCl_2$ or RPMI1640 media (1–2 × $10^7$ cells/ml). In some experiments (RNA-seq and chemokine microarrays), mouse neutrophils were further enriched using a neutrophil isolation kit (Miltenyi Biotec).

Human neutrophils were isolated using a Percoll density gradient as we described previously (Hahm et al., 2013; Li et al., 2020). Sodium citrate–treated human blood was mixed with an equal volume of 3% dextran and sedimented for 15 min. The supernatant (leukocytes-containing layer) was laid on the top of a discontinuous Percoll gradient (55% and 72%) and centrifuged at 370 *g* at 12°C for 1 h. The polymorphonuclear cells were collected at the interface of the two Percoll layers, resuspended with HBSS buffer, and then centrifuged at 300 *g* at 4°C for 10 min. After RBC lysis, neutrophils were resuspended as described above. Neutrophils were stimulated with a different concentration of fMLP or TNF-α for a different period at 37°C.

Washed human and mouse platelets were isolated as described previously (Kim et al., 2013). Platelets were adjusted to a density of 2 × $10^8$ cells/ml in Hepes–Tyrode buffer (20 mM Hepes, pH 7.4, 136 mM NaCl, 2.7 mM KCl, 12 mM $NaHCO_3$, 2 mM $MgCl_2$, and 5.5 mM glucose). Platelets were activated with 0.0125 U/ml thrombin for 5 min at 37°C. All healthy donors provided informed consent. The collection and use of blood samples for laboratory analysis were approved by the Institutional Review Board of the University of Illinois at Chicago and Washington University School of Medicine.

### Intravital microscopy

To induce peripheral vascular inflammation, WT, DREAM KO, or their BM chimeric mice were injected intrascrotally with murine TNF-α (500 ng) or MIP-2 (1 μg) as described previously (Hahm et al., 2013; Liu et al., 2007). 3 or 2 h after TNF-α or MIP-2 injection, respectively, mice were anesthetized by ketamine (125 mg/kg body weight [BW]) and xylazine (12.5 mg/kg BW). A tube was placed into the trachea, followed by cannulation of a jugular vein and exposure of the cremaster muscle. Neutrophils were monitored by infusion of Alexa Fluor 647–conjugated anti-Ly-6G antibodies (0.1 μg/g BW) into mice. In some experiments, superfusion buffer containing 10 μM fMLP was superfused on cremaster muscle in WT and DREAM KO mice at 37°C for 20, 40, and 60 min. Real-time images were captured in the inflamed cremaster venules with a diameter of 25–40 μm. The numbers of rolling, adherent, and transmigrated neutrophils were determined in an area of 0.02 $mm^2$ (number/field/5 min), followed by normalization to vessel length. Adherent neutrophils, defined as neutrophils that were stationary for >30 s and crawled but did not roll over, were counted. Five to seven different venules were monitored in one mouse. Fluorescently labeled (540/560) microspheres (diameter: 200 nm) were injected into mice, and the centerline velocity was calculated to assess blood flow rates. The experiments were performed in a single-blind manner. Fluorescence and bright-field images were recorded using either an Olympus BX61W microscope with a 60 × 1.0 numerical aperture (NA) water immersion objective or a Zeiss Axio examiner Z1 microscope system with a Yokogawa confocal spinning disk (CSU-W1) equipped with four-stack laser system (405 nm, 488 nm, 561 nm, and 637 nm wavelengths). Images were collected with a high-speed, high-resolution camera (2,304 × 2,304 pixel format; ORCA-Fusion BT sCMOS; Hamamatsu). Data were

analyzed using SlideBook, version 6.0 (Intelligent Imaging Innovations).

In some experiments, mice were treated with infusion of Alexa Fluor 647–conjugated anti-Ly-6G and DyLight 488–conjugated anti-CD42c antibodies (0.2 µg/g BW) to detect neutrophils and platelets, respectively. Neutrophils were monitored as described above. Adherent and accumulating platelets were quantified by the integrated median fluorescence intensity value of the anti-CD42c antibody. The antibody signal was normalized to the number of adherent neutrophils and the vessel length and plotted as a function of time.

For the adoptive transfer experiment, WT and DREAM KO neutrophils were isolated and labeled with a CellTracker Red CMTPX dye. The recipient WT and DREAM KO mice were treated with intrascrotal injection of TNF-α as described above. 3 h later, the labeled neutrophils ($10^6$ cells/0.1 ml/mouse) were injected into recipient mice through a femoral artery. Rolling, adhesion, and transmigration of infused neutrophils were counted.

In the experiment using chimeric mice with both WT (CD45.1) and DREAM KO (CD45.2) hematopoietic cells, the mice were treated with intrascrotal injection of TNF-α. 3 h later, Alexa Fluor 488–conjugated anti-mouse CD45.1, PE-conjugated anti-mouse CD45.2, and Alexa Fluor 647–conjugated anti-mouse Ly-6G antibodies were injected to evaluate the recruitment of WT and KO neutrophils on the inflamed cremaster endothelium as described above.

In some experiments, SCD, DREAM-deficient SCD, and their BM chimeric mice were treated with i.p. injection of TNF-α (500 ng). 3 h after TNF-α injection, neutrophils and platelets were visualized as described above. Rolling and adherent neutrophils were measured as described above. During or after intravital microscopic studies, the survival time of mice was recorded. Each time point began at TNF-α injection and ended when the mouse died or up to 8 h after TNF-α injection. In some experiments, WT and DREAM KO neutrophils were isolated and labeled with Calcein-AM or CellTracker Deep Red, respectively. The equal numbers of WT and KO neutrophils ($10^6$ each in 100 µl saline) were mixed and injected into TNF-α–challenged SCD mice. Rolling and adherent neutrophils were measured as described above.

### Immunohistochemistry

Following intravital microscopy, the cremaster muscle from each mouse was removed and cryosectioned after embedding in optimal cutting temperature compound. The tissues were sectioned with a thickness of 5 µm and then mounted on slides. The tissue sections were incubated with 1 µg/ml isotype control IgG, rat anti–ICAM-1, mouse anti–E-selectin, or mouse anti–P-selectin antibodies for 1 h, followed by incubation with 1 µg/ml DyLight 488–conjugated goat anti-rat IgG or anti-mouse IgG antibodies for 1 h. The sections were further labeled with 1 µg/ml APC-labeled rat anti-mouse PECAM-1 antibodies and mounted with Vectashield containing DAPI. Serial z-stack images (1 µm) were acquired using a laser scanning confocal microscope (LSM 510 META; Zeiss) equipped with 100×/1.30 NA oil objective lens and analyzed using the LSM Image Browser (v.4.2). Care was taken to image a given fluorochrome at the same settings for all experimental permutations. After merging the z-stack image slices into one, the mean fluorescence intensity (MFI) value of each antibody was calculated using ImageJ by outlining the endothelium. The average MFI value of control IgG was subtracted from that of each antibody. Multiple vessels (three or four vessels/mouse) were analyzed from three to six mice per group.

### Flow chamber assay

Flow chamber assays under venous shear were performed as we described (Hahm et al., 2013). Confluent C57BL/6 mouse primary pulmonary vein ECs (Cell Biologics) on Fg-coated glass coverslips were stimulated with 20 ng/ml TNF-α for 6 h and placed into a parallel plate flow chamber (Bioptech). The chamber temperature was maintained at 37°C using a temperature controller. Neutrophils, $3 \times 10^6$, were treated with 20 ng/ml TNF-α or 10 µM fMLP for 10 min. After washing, neutrophils were perfused for 10 min over activated ECs under venous shear of 1 dyne/cm$^2$. Then the medium was perfused for 5 min to wash out weakly bound cells. Images were obtained using a Nikon microscope (ECLIPSE Ti) with a 10×/0.25 NA objective lens and were recorded with a camera (CoolSNAP ES2). The data were analyzed using NIS Elements (AR 3.2). Rolling, adherent, and transmigrated neutrophils were counted in a field of 0.15 mm$^2$. The number of adherent neutrophils was additionally counted in four different regions.

### Chemokine microarray

WT and DREAM KO neutrophils ($5 \times 10^7$ cells/ml) were treated with or without 10 ng/ml TNF-α at 37°C for 3 h. The cell suspension was lysed with 2× lysis buffer (2% IGEPAL CA-630, 20 mM Tris-HCl, pH 8.0, 137 mM NaCl, 10% glycerol, 2 mM EDTA, and protease inhibitor cocktail). After the bicinchoninic acid protein assay, an equal amount of protein (550 µg) was used for the mouse chemokine microarray (ARY020; R&D Systems) according to the manufacturer's instructions.

### RNA-seq

Mouse BM neutrophils were enriched using a mouse neutrophil isolation kit (Miltenyi Biotec). Total RNAs were isolated using the RNeasy Plus Mini Kit (Qiagen), and 300 ng of total RNA was used to generate the RNA-seq library using the NEBNext Ultra II RNA Library Prep with Sample Purification Beads (NEB) according to the manufacturer's instructions. Briefly, mRNAs were isolated from total RNAs with the NEBNext Poly(A) mRNA Magnetic Isolation Module (NEB), fragmented, and primed. First-strand cDNAs were synthesized, following by second-strand synthesis. The ends of purified double-strand cDNAs were repaired, ligated with an adaptor, and amplified with barcoded primers (NEBNext Multiplex Oligos for Illumina) using PCR. The purified final PCR product was sequenced using Illumina NovaSeq 6000. The reads were aligned to the mouse transcriptome (mm10) using a default setting of STAR (v.020201). Aligned reads were counted using HTseq (v.0.6.1p1). GSEA was performed using inflammation-related gene sets (positive regulation of inflammatory response (gene ontology [GO]: 0050729)

and negative regulation of inflammatory response (GO:0050728)) obtained from the GO database. The Gene Expression Omnibus accession no. is GSE172394.

### ChIP analysis

ChIP assays were performed as described previously (Aggarwal, 1990). Briefly, mouse neutrophils ($2 \times 10^8$ cells in 20 ml RPMI1640 media) were cross-linked with 1% formaldehyde for 7 min at room temperature. After quenching with 125 mM glycine, cells were washed with PBS and resuspended in ChIP dilution buffer (20 mM Tris-HCl, pH 8.1, containing 1% Triton X-100, 2 mM EDTA, 150 mM NaCl, 0.1% SDS, and protease inhibitor cocktail) and sonicated using a Bioruptor (Diagenode) with a setting of 30 s on and 1 min off for 10 min (three times). Cell lysates containing an average size of 300 bp DNA were immunoprecipitated with 10 µg of polyclonal anti-DREAM antibodies (Sigma-Aldrich) to enrich DREAM-DNA complexes. RT-qPCRs were performed using PerfeCTa SYBR Green FastMix (Quanta) with StepOnePlus real-time PCR machine (Applied Biosystems). The following primers were used: mTnfaip3 DRE1 forward: 5′-TGCACTGCATCCAACCTGAA-3′ and reverse: 5′-AAATCGCGGTGATGGGAACT-3′; mTnfaip3 DRE2 forward: 5′-GTTCCCATCACCGCGATTTC-3′ and reverse: 5′-GGAGCATCG CTCACCTCTTG-3′; mTnfaip3 DRE3 forward: 5′-CCCGGAGAA ACTCCTAGGTC-3′ and reverse: 5′-CATTTCCAGTTCCCATCA CC-3′; and mGfi1b (control) forward: 5′-CCCGGAGAAACTCCT AGGTC-3′ and reverse: 5′-CATTTCCAGTTCCCATCACC-3′. Cycle threshold (Ct) values of the ChIP sample and control were normalized against the Gfi1b proximal promoter binding site as a loading control. The relative fold enrichment was calculated using ΔΔ Ct values.

### RT-qPCR

RNAs were isolated from HUVECs and human neutrophils with the RNeasy Plus mini kit (Qiagen) and used to generate cDNA with the RevertAid First Strand cDNA Synthesis Kit (Thermo Fisher Scientific), followed by RT-PCR with FastStart Universal SYBR Green Master (Rox; Sigma-Aldrich) in the ViiA 7 Real-Time PCR System (Thermo Fisher Scientific). The region between exon 4 and exon 5 of DREAM was amplified using primers (forward: 5′-CTTTGAGGACTTTGTGGTTGGCC-3′; reverse: 5′-CATCTCCTCTTTGGTGATGTAGCC-3′). Human GAPDH was used to compare the cDNA amount (forward: 5′-GTCTCCTCTGACTTC AACAGCG-3′; reverse: 5′-ACCACCCTGTTGCTGTAGCCAA-3′). Δ Ct values were calculated using the GAPDH Ct values for each sample.

### Glutathione *S*-transferase (GST)–tagged human DREAM

Human DREAM cDNAs were generated from IDT, cloned into EcoRI and Xhol restriction sites in pGEX-6P-1 (Addgene), and expressed in BL21 cells. GST-tagged human DREAM was purified using glutathione-conjugated Sepharose beads (GE Healthcare Life Sciences).

### DREAM knockdown in HL-60 cells

Human embryonic kidney and HL-60 cells (American Type Culture Collection) were cultured in DMEM (4.5 g/liter glucose) and RPMI1640 media, respectively, with a supplement of 10% fetal bovine serum. To produce lentiviruses, DNA constructs with scrambled or human DREAM shRNA were transfected into human embryonic kidney cells using Lipofectamine 2000 according to the manufacturer's instructions. Lentiviral particles were collected 72 h after transfection. For lentiviral infection, HL-60 cells were spinoculated twice at 2,000 rpm for 2 h in the presence of 8 µg/ml polybrene. Cells were then cultured in RPMI1640 media containing 5 µg/ml puromycin. 2 wk later, DREAM knockdown was confirmed by immunoblotting. HL-60 cells with DREAM knockdown ($2 \times 10^5$ cells/ml) were differentiated into human neutrophil-like cells (dHL-60) by the addition of 1.3% DMSO to the media for 5–7 d before experiments.

### Flow cytometry

WT and DREAM KO neutrophils, human neutrophils, or dHL-60 cells, $2.5 \times 10^5$/100 µl, were treated with fMLP or TNF-α. In some experiments, cells were pretreated with a different concentration of TPCA-1 or Bay 11–7082 for 15 min at 37°C. Cells were labeled using fluorescently labeled antibodies against cell surface molecules or control IgGs. For Fg binding assays, neutrophils were treated with 0.5 mM $MnCl_2$ for 2 min at room temperature and incubated with 10 µg/ml DyLight 488–labeled Fg for 4 min at room temperature. Neutrophils were then stimulated with fMLP or TNF-α at 37°C. In some experiments, human neutrophils were pretreated with a different concentration of TPCA-1 for 15 min at 37°C and stimulated with fMLP or TNF-α. Cells were labeled with fluorescently labeled antibodies against αMβ2 or αLβ2 integrin. Flow-cytometric analysis was performed using a Cyan-ADP or CytoFlex flow cytometer (Beckman Coulter). Data were presented as the geometric MFI value.

### Neutrophil adhesion assay

Glass coverslips were coated with 10 µg/ml mouse ICAM-1. WT and DREAM KO neutrophils were suspended in HBSS buffer (20 mM Hepes, pH 7.4, containing 1 mM $MgCl_2$), and $5 \times 10^5$ cells (in 400 µl) were plated on immobilized ICAM-1 in the presence or absence of 10 ng/ml TNF-α or 10 µM fMLP for 20 min at 37°C as we described previously (Hahm et al., 2013). Adherent neutrophils were counted in a field of 0.033 $mm^2$ (five separate fields/experiment) under a microscope.

### β2-talin1 binding

β2-talin1 binding was measured as described previously (Li et al., 2014). Mouse neutrophils ($4 \times 10^6$/400 µl) were treated with or without fMLP for 1 min or TNF-α for 2 min. Human neutrophils ($4 \times 10^6$/400 µl) were treated with or without 0.3 µM TPCA-1 for 15 min at 37°C and stimulated with TNF-α for 2 min. Cells were then lysed with a lysis buffer (20 mM Hepes, pH 7.4, containing 1.5% NP-40, 1.5% 3-(3-cholamidopropyl)diethylammonio-1 propanesulfonate, 0.5% sodium deoxycholate, 150 mM NaCl, proteinase inhibitor cocktail, 1 mM PMSF, 1 mM $Na_3VO_4$ and 1 mM NaF) on ice. Lysates were incubated with control IgG or anti-β2 antibodies, followed by incubation with protein A/G agarose beads. Immunoblotting was performed

using anti-talin1 antibodies, and the band density of talin1 was normalized to that of β2.

### ROS production

The wells of a 96-well plate were coated with 250 µg/ml human Fg in 50 mM carbonate-bicarbonate buffer, pH 9.6, at 4°C overnight. WT and KO neutrophils (2 × $10^5$/100 µl) in HBSS buffer (20 mM Hepes, pH 7.4, containing 1 mM $CaCl_2$ and 0.5 mM $MgCl_2$) mixed with 125 µM luminol and 10 U/ml horseradish peroxidase were added to the wells and incubated at 37°C for 15 min. After the addition of 20 ng/ml TNF-α or 10 µM fMLP, light emission was recorded every 20 s using a SpectraMax L microplate reader (Molecular Devices) at 37°C for 40 min.

### Degranulation assay

To evaluate the degranulation of specific/gelatinase granules, WT or DREAM KO neutrophils, 2 × $10^6$/100 µl, were incubated with vehicle (0.1% DMSO) or a different concentration of TPCA-1 or Bay 11–7082 for 15 min at 37°C, washed, and resuspended in RPMI1640 media. In some experiments, dHL-60 cells (2 × $10^6$/100 µl) transfected with control or DREAM shRNA were used. After stimulation with fMLP or TNF-α for 10 min, cells were centrifuged. The supernatant, 100 µl, was used to measure gelatinase activity using the EnzChek Gelatinase/Collagenase Assay Kit (Thermo Fisher Scientific). The fluorescence intensity was measured on a PHERAstar plate reader (BMG Labtech) with excitation wavelength at 485 nm and emission wavelength at 520 nm. Data were presented as total activity using known concentrations of collagenase as a standard curve. To measure the degranulation of azurophilic granules, WT or DREAM KO neutrophils (2 × $10^7$ in 100 µl) in HBSS buffer containing 1 mM $CaCl_2$ and 1 mM $MgCl_2$ were stimulated with 10 µM fMLP or 5 ng/ml TNF-α for 10 min at 37°C. The supernatant was collected and incubated with 0.3 mM $H_2O_2$ and 10.5% 3,3′,5,5′-tetramethylbenzidine solution (Thermo Fisher Scientific) to detect the activity of MPO. The reaction was quenched with the addition of 0.8 N HCl, and the absorbance was read on a PHERAstar plate reader at 450 nm.

### Phosphorylation of IKKβ or SNAP-23

Mouse and human neutrophils, 2 × $10^7$/ml, were pretreated with vehicle, TPCA-1, or Bay 11–7082 for 15 min at 37°C and then stimulated with TNF-α for 0–20 min at 37°C. For the detection of pIKKα/β, equal amounts (50 µg protein) of cell lysates were used for immunoblotting. For the detection of phosphorylated SNAP-23, cell lysates were incubated with control IgG or anti–SNAP-23 antibodies, followed by incubation with protein A/G agarose beads. The bound fraction was immunoblotted using antibodies against phosphoSer, pIKKα/β, or SNAP-23. Densitometric analysis was performed using ImageJ.

### In vitro heterotypic neutrophil-platelet aggregation

Platelets (2 × $10^7$) and neutrophils ($10^6$) isolated from WT and DREAM KO mice were labeled with DyLight 488–conjugated anti-CD42c and Alexa Fluor 647–conjugated anti–Ly-6G antibodies, respectively. Isolated human neutrophils and platelets were labeled with APC-conjugated anti-CD41 and FITC-conjugated anti–L-selectin antibodies, respectively. The antibody-stained cells were pretreated with vehicle or 0.3 µM TPCA-1, or 10 µg/ml control IgG or a blocking anti–P-selectin antibody. Neutrophils were stimulated with 5 ng/ml TNF-α for 5 min. Platelets were treated with 0.0125 U/ml thrombin for 5 min at 37°C, followed by incubation with 50 µM D-Phe-Pro-Arg-chloromethylketone. Activated platelets were mixed with stimulated neutrophils under a stirring condition of 1,000 rpm in an aggregometer. After a 5-min incubation, cells were fixed and analyzed by flow cytometry. Data were presented as the percentage of the number of cell–cell aggregates in the R1 gate or the geometric MFI value of anti-CD42c or anti-CD41 antibodies (heterotypic interaction) normalized to a control group (WT platelets/neutrophils or control IgG-treated cells) as we described (Li et al., 2014). The number of cell–cell aggregates and the fluorescence signal of the anti-CD42c antibody in WT platelets and WT neutrophils were shown as 100%.

For immunofluorescence microscopy, fixed cell aggregates were cytospun at 800 *g* for 5 min and mounted to slides with Vectashield Antifade mounting medium containing DAPI. Fluorescence images were obtained with a Nikon microscope (ECLIPSE Ti) equipped with a Plan Fluor × 40/1.30 NA oil objective lens and a digital camera (CoolSNAP ES2). The data were analyzed using NIS-Elements (AR 3.2; Nikon).

### Statistics

Data were analyzed using GraphPad Prism v9.0.2 by Student's *t* test, Mann–Whitney *U* test, ANOVA with Dunnett's or Tukey's test, Kruskal–Wallis test with post hoc Dunn's test, and Mantle–Cox log-rank test. A P value <0.05 was considered significant.

### Online supplemental material

Fig. S1 shows that DREAM does not regulate P-selectin expression on the TNF-α–inflamed endothelium. Fig. S2 and Fig. S3 provide control data showing the purity of isolated mouse and human neutrophils and the expression of surface molecules in WT and DREAM KO neutrophils. Fig. S4 suggests the role of neutrophil DREAM in ROS production after stimulation with TNF-α. Fig. S5 provides data showing the genotyping and complete blood counts of SCD mice and nonhematopoietic and/or hematopoietic DREAM-deficient SCD mice. Table S1 shows the number of circulating blood cells in WT and DREAM KO mice, and Table S2 shows the number of circulating blood cells in control and DREAM BM chimeric mice. Table S3 provides RNA-seq data of WT and DREAM KO neutrophils following TNF-α stimulation. Video 1 shows neutrophil recruitment during TNF-α–induced cremaster venular inflammation in WT mice. Video 2 shows neutrophil recruitment during TNF-α–induced cremaster venular inflammation in DREAM KO mice. Video 3 shows recruitment of WT and DREAM KO neutrophils during TNF-α–induced cremaster venular inflammation. Video 4 shows recruitment of WT neutrophils on a monolayer of TNF-α–inflamed ECs. Video 5 shows recruitment of DREAM KO neutrophils on a monolayer of TNF-α–inflamed ECs. Video 6 shows neutrophil–platelet interactions during TNF-α–induced

cremaster venular inflammation in WT mice. Video 7 shows Neutrophil–platelet interactions during TNF-α–induced cremaster venular inflammation in DREAM KO mice.

## Acknowledgments

The authors thank Dr. Josef Penninger (University of British Columbia, Vancouver, Canada) for providing DREAM KO mice and Dr. Chinnaswamy Tiruppathi for his helpful comments.

This work was supported by the National Institutes of Health grants HL125838 (to B. Razani); GM112722 and HD101512 (to J. Kim); HL140837 (to M.C. Dinauer); and HL153047, HL130028, HL148280, and HL146559 (to J. Cho), and by VA Merit Review grant BX003415 (to B. Razani). J. Li is a recipient of the American Heart Association Career Development Award (18CDA34110402).

Author contributions: J. Li, T. Kumari, and A. Barazia designed and performed the experiments, collected and analyzed data, and wrote a draft of the manuscript; V. Jha, S.Y. Jeong, A. Olson, M. Kim, B.K. Lee, V. Manickam, Z. Song, and J. Kim performed the experiments and analyzed data; R. Clemens, B. Razani, and M.C. Dinauer provided important reagents and comments; and J. Cho initiated research, oversaw all experiments and data interpretation, and wrote the manuscript.

Disclosures: The authors declare no competing interests exist.

Submitted: 18 May 2021
Revised: 21 September 2021
Accepted: 19 October 2021

## References

Aggarwal, B.B. 1990. Lymphotoxin and tumor necrosis factor: qualitative and quantitative differences in their receptors and signal transduction in various cell types. *Prog. Clin. Biol. Res.* 349:375–384.

Arnaout, M.A. 2016. Biology and structure of leukocyte $\beta_2$ integrins and their role in inflammation. *F1000 Res.* 5:2433. https://doi.org/10.12688/f1000research.9415.1

Ataga, K.I., A. Kutlar, J. Kanter, D. Liles, R. Cancado, J. Friedrisch, T.H. Guthrie, J. Knight-Madden, O.A. Alvarez, V.R. Gordeuk, et al. 2017. Crizanlizumab for the Prevention of Pain Crises in Sickle Cell Disease. *N. Engl. J. Med.* 376:429–439. https://doi.org/10.1056/NEJMoa1611770

Barazia, A., J. Li, K. Kim, N. Shabrani, and J. Cho. 2015. Hydroxyurea with AKT2 inhibition decreases vaso-occlusive events in sickle cell disease mice. *Blood.* 126:2511–2517. https://doi.org/10.1182/blood-2015-02-626234

Boone, D.L., E.E. Turer, E.G. Lee, R.C. Ahmad, M.T. Wheeler, C. Tsui, P. Hurley, M. Chien, S. Chai, O. Hitotsumatsu, et al. 2004. The ubiquitin-modifying enzyme A20 is required for termination of Toll-like receptor responses. *Nat. Immunol.* 5:1052–1060. https://doi.org/10.1038/ni1110

Borregaard, N., L. Kjeldsen, H. Sengeløv, M.S. Diamond, T.A. Springer, H.C. Anderson, T.K. Kishimoto, and D.F. Bainton. 1994. Changes in subcellular localization and surface expression of L-selectin, alkaline phosphatase, and Mac-1 in human neutrophils during stimulation with inflammatory mediators. *J. Leukoc. Biol.* 56:80–87. https://doi.org/10.1002/jlb.56.1.80

Buxbaum, J.D., E.K. Choi, Y. Luo, C. Lilliehook, A.C. Crowley, D.E. Merriam, and W. Wasco. 1998. Calsenilin: a calcium-binding protein that interacts with the presenilins and regulates the levels of a presenilin fragment. *Nat. Med.* 4:1177–1181. https://doi.org/10.1038/2673

Cabal-Hierro, L., and P.S. Lazo. 2012. Signal transduction by tumor necrosis factor receptors. *Cell. Signal.* 24:1297–1305. https://doi.org/10.1016/j.cellsig.2012.02.006

Calì, T., L. Fedrizzi, D. Ottolini, R. Gomez-Villafuertes, B. Mellström, J.R. Naranjo, E. Carafoli, and M. Brini. 2012. Ca2+-activated nucleotidase 1, a novel target gene for the transcriptional repressor DREAM (downstream regulatory element antagonist modulator), is involved in protein folding and degradation. *J. Biol. Chem.* 287:18478–18491. https://doi.org/10.1074/jbc.M111.304733

Chang, J., J.T. Patton, A. Sarkar, B. Ernst, J.L. Magnani, and P.S. Frenette. 2010. GMI-1070, a novel pan-selectin antagonist, reverses acute vascular occlusions in sickle cell mice. *Blood.* 116:1779–1786. https://doi.org/10.1182/blood-2009-12-260513

Cheng, H.Y., G.M. Pitcher, S.R. Laviolette, I.Q. Whishaw, K.I. Tong, L.K. Kockeritz, T. Wada, N.A. Joza, M. Crackower, J. Goncalves, et al. 2002. DREAM is a critical transcriptional repressor for pain modulation. *Cell.* 108:31–43. https://doi.org/10.1016/S0092-8674(01)00629-8

Cho, J., J.L. Degen, B.S. Coller, and D.F. Mosher. 2005. Fibrin but not adsorbed fibrinogen supports fibronectin assembly by spread platelets. Effects of the interaction of alphaIIb beta3 with the C terminus of the fibrinogen gamma-chain. *J. Biol. Chem.* 280:35490–35498. https://doi.org/10.1074/jbc.M506289200

Craig, T.A., P.L. Ramachandran, H.R. Bergen III, J.L. Podratz, A.J. Windebank, and R. Kumar. 2013. The regulation of apoptosis by the downstream regulatory element antagonist modulator/potassium channel interacting protein 3 (DREAM/KChIP3) through interactions with hexokinase I. *Biochem. Biophys. Res. Commun.* 433:508–512. https://doi.org/10.1016/j.bbrc.2013.03.016

Gómez-Moreno, D., J.M. Adrover, and A. Hidalgo. 2018. Neutrophils as effectors of vascular inflammation. *Eur. J. Clin. Invest.* 48(Suppl 2):e12940. https://doi.org/10.1111/eci.12940

Gonzalez, W.G., A.S. Arango, and J. Miksovska. 2015. Amphiphilic Residues 29-44 of DREAM N-Termini Mediate Calmodulin:DREAM Complex Formation. *Biochemistry.* 54:4391–4403. https://doi.org/10.1021/acs.biochem.5b00251

Hahm, E., J. Li, K. Kim, S. Huh, S. Rogelj, and J. Cho. 2013. Extracellular protein disulfide isomerase regulates ligand-binding activity of αMβ2 integrin and neutrophil recruitment during vascular inflammation. *Blood.* 121:3789–3800: S1–S15. https://doi.org/10.1182/blood-2012-11-467985

Hayden, M.S., and S. Ghosh. 2011. NF-κB in immunobiology. *Cell Res.* 21:223–244. https://doi.org/10.1038/cr.2011.13

Hepp, R., N. Puri, A.C. Hohenstein, G.L. Crawford, S.W. Whiteheart, and P.A. Roche. 2005. Phosphorylation of SNAP-23 regulates exocytosis from mast cells. *J. Biol. Chem.* 280:6610–6620. https://doi.org/10.1074/jbc.M412126200

Jang, J.E., A. Hidalgo, and P.S. Frenette. 2012. Intravenous immunoglobulins modulate neutrophil activation and vascular injury through FcγRIII and SHP-1. *Circ. Res.* 110:1057–1066. https://doi.org/10.1161/CIRCRESAHA.112.266411

Karim, Z.A., J. Zhang, M. Banerjee, M.C. Chicka, R. Al Hawas, T.R. Hamilton, P.A. Roche, and S.W. Whiteheart. 2013. IκB kinase phosphorylation of SNAP-23 controls platelet secretion. *Blood.* 121:4567–4574. https://doi.org/10.1182/blood-2012-11-470468

Kim, K., E. Hahm, J. Li, L.M. Holbrook, P. Sasikumar, R.G. Stanley, M. Ushio-Fukai, J.M. Gibbins, and J. Cho. 2013. Platelet protein disulfide isomerase is required for thrombus formation but not for hemostasis in mice. *Blood.* 122:1052–1061. https://doi.org/10.1182/blood-2013-03-492504

Kim, K., J. Li, A. Tseng, R.K. Andrews, and J. Cho. 2015. NOX2 is critical for heterotypic neutrophil-platelet interactions during vascular inflammation. *Blood.* 126:1952–1964. https://doi.org/10.1182/blood-2014-10-605261

Kim, K., J. Li, A. Barazia, A. Tseng, S.W. Youn, G. Abbadessa, Y. Yu, B. Schwartz, R.K. Andrews, V.R. Gordeuk, and J. Cho. 2017a. ARQ 092, an orally-available, selective AKT inhibitor, attenuates neutrophil-platelet interactions in sickle cell disease. *Haematologica.* 102:246–259. https://doi.org/10.3324/haematol.2016.151159

Kim, K., A. Tseng, A. Barazia, J.E. Italiano, and J. Cho. 2017b. DREAM plays an important role in platelet activation and thrombogenesis. *Blood.* 129:209–225. https://doi.org/10.1182/blood-2016-07-724419

Konstantopoulos, K., S. Neelamegham, A.R. Burns, E. Hentzen, G.S. Kansas, K.R. Snapp, E.L. Berg, J.D. Hellums, C.W. Smith, L.V. McIntire, and S.I. Simon. 1998. Venous levels of shear support neutrophil-platelet adhesion and neutrophil aggregation in blood via P-selectin and beta2-integrin. *Circulation.* 98:873–882. https://doi.org/10.1161/01.CIR.98.9.873

Lefort, C.T., J. Rossaint, M. Moser, B.G. Petrich, A. Zarbock, S.J. Monkley, D.R. Critchley, M.H. Ginsberg, R. Fässler, and K. Ley. 2012. Distinct roles for

talin-1 and kindlin-3 in LFA-1 extension and affinity regulation. *Blood.* 119:4275–4282. https://doi.org/10.1182/blood-2011-08-373118

Li, Q., and I.M. Verma. 2002. NF-kappaB regulation in the immune system. *Nat. Rev. Immunol.* 2:725–734. https://doi.org/10.1038/nri910

Li, J., K. Kim, E. Hahm, R. Molokie, N. Hay, V.R. Gordeuk, X. Du, and J. Cho. 2014. Neutrophil AKT2 regulates heterotypic cell-cell interactions during vascular inflammation. *J. Clin. Invest.* 124:1483–1496. https://doi.org/10.1172/JCI72305

Li, J., K. Kim, A. Barazia, A. Tseng, and J. Cho. 2015. Platelet-neutrophil interactions under thromboinflammatory conditions. *Cell. Mol. Life Sci.* 72: 2627–2643. https://doi.org/10.1007/s00018-015-1845-y

Li, J., K. Kim, S.Y. Jeong, J. Chiu, B. Xiong, P.A. Petukhov, X. Dai, X. Li, R.K. Andrews, X. Du, et al. 2019. Platelet protein disulfide isomerase promotes glycoprotein Ibalpha-mediated platelet-neutrophil interactions under thromboinflammatory conditions. *Circulation.* 139:1300–1319. https://doi.org/10.1161/CIRCULATIONAHA.118.036323

Li, J., S.Y. Jeong, B. Xiong, A. Tseng, A.B. Mahon, S. Isaacman, V.R. Gordeuk, and J. Cho. 2020. Repurposing pyridoxamine for therapeutic intervention of intravascular cell-cell interactions in mouse models of sickle cell disease. *Haematologica.* 105:2407–2419.

Ling, L., Z. Cao, and D.V. Goeddel. 1998. NF-kappaB-inducing kinase activates IKK-alpha by phosphorylation of Ser-176. *Proc. Natl. Acad. Sci. USA.* 95: 3792–3797. https://doi.org/10.1073/pnas.95.7.3792

Linnerz, T., and C.J. Hall. 2020. The Diverse Roles of Phagocytes During Bacterial and Fungal Infections and Sterile Inflammation: Lessons From Zebrafish. *Front. Immunol.* 11:1094. https://doi.org/10.3389/fimmu.2020.01094

Liu, L., K.D. Puri, J.M. Penninger, and P. Kubes. 2007. Leukocyte PI3Kgamma and PI3Kdelta have temporally distinct roles for leukocyte recruitment in vivo. *Blood.* 110:1191–1198. https://doi.org/10.1182/blood-2006-11-060103

Logan, M.R., S.O. Odemuyiwa, and R. Moqbel. 2003. Understanding exocytosis in immune and inflammatory cells: the molecular basis of mediator secretion. *J. Allergy Clin. Immunol.* 111:923–932, quiz: 933. https://doi.org/10.1016/S0091-6749(03)80114-8

Lominadze, G., D.W. Powell, G.C. Luerman, A.J. Link, R.A. Ward, and K.R. McLeish. 2005. Proteomic analysis of human neutrophil granules. *Mol. Cell. Proteomics.* 4:1503–1521. https://doi.org/10.1074/mcp.M500143-MCP200

Maelfait, J., K. Roose, P. Bogaert, M. Sze, X. Saelens, M. Pasparakis, I. Carpentier, G. van Loo, and R. Beyaert. 2012. A20 (Tnfaip3) deficiency in myeloid cells protects against influenza A virus infection. *PLoS Pathog.* 8:e1002570. https://doi.org/10.1371/journal.ppat.1002570

Martín-Martín, B., S.M. Nabokina, J. Blasi, P.A. Lazo, and F. Mollinedo. 2000. Involvement of SNAP-23 and syntaxin 6 in human neutrophil exocytosis. *Blood.* 96:2574–2583. https://doi.org/10.1182/blood.V96.7.2574

Mazo, I.B., S. Massberg, and U.H. von Andrian. 2011. Hematopoietic stem and progenitor cell trafficking. *Trends Immunol.* 32:493–503. https://doi.org/10.1016/j.it.2011.06.011

McDonald, P.P., A. Bald, and M.A. Cassatella. 1997. Activation of the NF-kappaB pathway by inflammatory stimuli in human neutrophils. *Blood.* 89:3421–3433. https://doi.org/10.1182/blood.V89.9.3421

McEver, R.P. 2015. Selectins: initiators of leucocyte adhesion and signalling at the vascular wall. *Cardiovasc. Res.* 107:331–339. https://doi.org/10.1093/cvr/cvv154

Mellström, B., I. Sahún, A. Ruiz-Nuño, P. Murtra, R. Gomez-Villafuertes, M. Savignac, J.C. Oliveros, P. Gonzalez, A. Kastanauskaite, S. Knafo, et al. 2014. DREAM controls the on/off switch of specific activity-dependent transcription pathways. *Mol. Cell. Biol.* 34:877–887. https://doi.org/10.1128/MCB.00360-13

Mercurio, F., H. Zhu, B.W. Murray, A. Shevchenko, B.L. Bennett, J. Li, D.B. Young, M. Barbosa, M. Mann, A. Manning, and A. Rao. 1997. IKK-1 and IKK-2: cytokine-activated IkappaB kinases essential for NF-kappaB activation. *Science.* 278:860–866. https://doi.org/10.1126/science.278.5339.860

Montecucco, F., S. Steffens, F. Burger, A. Da Costa, G. Bianchi, M. Bertolotto, F. Mach, F. Dallegri, and L. Ottonello. 2008. Tumor necrosis factor-alpha (TNF-alpha) induces integrin CD11b/CD18 (Mac-1) up-regulation and migration to the CC chemokine CCL3 (MIP-1alpha) on human neutrophils through defined signalling pathways. *Cell. Signal.* 20: 557–568. https://doi.org/10.1016/j.cellsig.2007.11.008

Nasimuzzaman, M., P.I. Arumugam, E.S. Mullins, J.M. James, K. Vanden-Heuvel, M.G. Narciso, M.A. Shaw, S. McGraw, B.J. Aronow, and P. Malik. 2019. Elimination of the fibrinogen integrin $\alpha_M\beta_2$-binding motif improves renal pathology in mice with sickle cell anemia. *Blood Adv.* 3: 1519–1532. https://doi.org/10.1182/bloodadvances.2019032342

Phillipson, M., and P. Kubes. 2011. The neutrophil in vascular inflammation. *Nat. Med.* 17:1381–1390. https://doi.org/10.1038/nm.2514

Phillipson, M., B. Heit, P. Colarusso, L. Liu, C.M. Ballantyne, and P. Kubes. 2006. Intraluminal crawling of neutrophils to emigration sites: a molecularly distinct process from adhesion in the recruitment cascade. *J. Exp. Med.* 203:2569–2575. https://doi.org/10.1084/jem.20060925

Podolin, P.L., J.F. Callahan, B.J. Bolognese, Y.H. Li, K. Carlson, T.G. Davis, G.W. Mellor, C. Evans, and A.K. Roshak. 2005. Attenuation of murine collagen-induced arthritis by a novel, potent, selective small molecule inhibitor of IkappaB Kinase 2, TPCA-1 (2-[(aminocarbonyl)amino]-5-(4-fluorophenyl)-3-thiophenecarboxamide), occurs via reduction of proinflammatory cytokines and antigen-induced T cell Proliferation. *J. Pharmacol. Exp. Ther.* 312:373–381. https://doi.org/10.1124/jpet.104.074484

Rauert-Wunderlich, H., D. Siegmund, E. Maier, T. Giner, R.C. Bargou, H. Wajant, and T. Stühmer. 2013. The IKK inhibitor Bay 11-7082 induces cell death independent from inhibition of activation of NFκB transcription factors. *PLoS One.* 8:e59292. https://doi.org/10.1371/journal.pone.0059292

Salzmann, M., S. Bleichert, B. Moser, M. Mussbacher, M. Haase, B. Hoesel, W.C. Schrottmaier, J.B. Kral-Pointner, M. Itakura, K. Schmidt, et al. 2020. IκB kinase 2 is not essential for platelet activation. *Blood Adv.* 4: 638–643. https://doi.org/10.1182/bloodadvances.2019001044

Skaug, B., J. Chen, F. Du, J. He, A. Ma, and Z.J. Chen. 2011. Direct, noncatalytic mechanism of IKK inhibition by A20. *Mol. Cell.* 44:559–571. https://doi.org/10.1016/j.molcel.2011.09.015

Tiruppathi, C., D. Soni, D.M. Wang, J. Xue, V. Singh, P.B. Thippegowda, B.P. Cheppudira, R.K. Mishra, A. Debroy, Z. Qian, et al. 2014. The transcription factor DREAM represses the deubiquitinase A20 and mediates inflammation. *Nat. Immunol.* 15:239–247. https://doi.org/10.1038/ni.2823

Turhan, A., L.A. Weiss, N. Mohandas, B.S. Coller, and P.S. Frenette. 2002. Primary role for adherent leukocytes in sickle cell vascular occlusion: a new paradigm. *Proc. Natl. Acad. Sci. USA.* 99:3047–3051. https://doi.org/10.1073/pnas.052522799

Wertz, I.E., K.M. O'Rourke, H. Zhou, M. Eby, L. Aravind, S. Seshagiri, P. Wu, C. Wiesmann, R. Baker, D.L. Boone, et al. 2004. De-ubiquitination and ubiquitin ligase domains of A20 downregulate NF-kappaB signalling. *Nature.* 430:694–699. https://doi.org/10.1038/nature02794

Wolf, D., N. Anto-Michel, H. Blankenbach, A. Wiedemann, K. Buscher, J.D. Hohmann, B. Lim, M. Bäuml, A. Marki, M. Mauler, et al. 2018. A ligand-specific blockade of the integrin Mac-1 selectively targets pathologic inflammation while maintaining protective host-defense. *Nat. Commun.* 9:525. https://doi.org/10.1038/s41467-018-02896-8

Xu, J., F. Wang, A. Van Keymeulen, P. Herzmark, A. Straight, K. Kelly, Y. Takuwa, N. Sugimoto, T. Mitchison, and H.R. Bourne. 2003. Divergent signals and cytoskeletal assemblies regulate self-organizing polarity in neutrophils. *Cell.* 114:201–214. https://doi.org/10.1016/S0092-8674(03)00555-5

Ye, F., C. Kim, and M.H. Ginsberg. 2011. Molecular mechanism of inside-out integrin regulation. *J. Thromb. Haemost.* 9(suppl 1):20–25. https://doi.org/10.1111/j.1538-7836.2011.04355.x

Zarbock, A., K. Ley, R.P. McEver, and A. Hidalgo. 2011. Leukocyte ligands for endothelial selectins: specialized glycoconjugates that mediate rolling and signaling under flow. *Blood.* 118:6743–6751. https://doi.org/10.1182/blood-2011-07-343566

Zhang, D., C. Xu, D. Manwani, and P.S. Frenette. 2016. Neutrophils, platelets, and inflammatory pathways at the nexus of sickle cell disease pathophysiology. *Blood.* 127:801–809. https://doi.org/10.1182/blood-2015-09-618538

Zhang, Q., M.J. Lenardo, and D. Baltimore. 2017. 30 Years of NF-κB: A Blossoming of Relevance to Human Pathobiology. *Cell.* 168:37–57. https://doi.org/10.1016/j.cell.2016.12.012

## Supplemental material

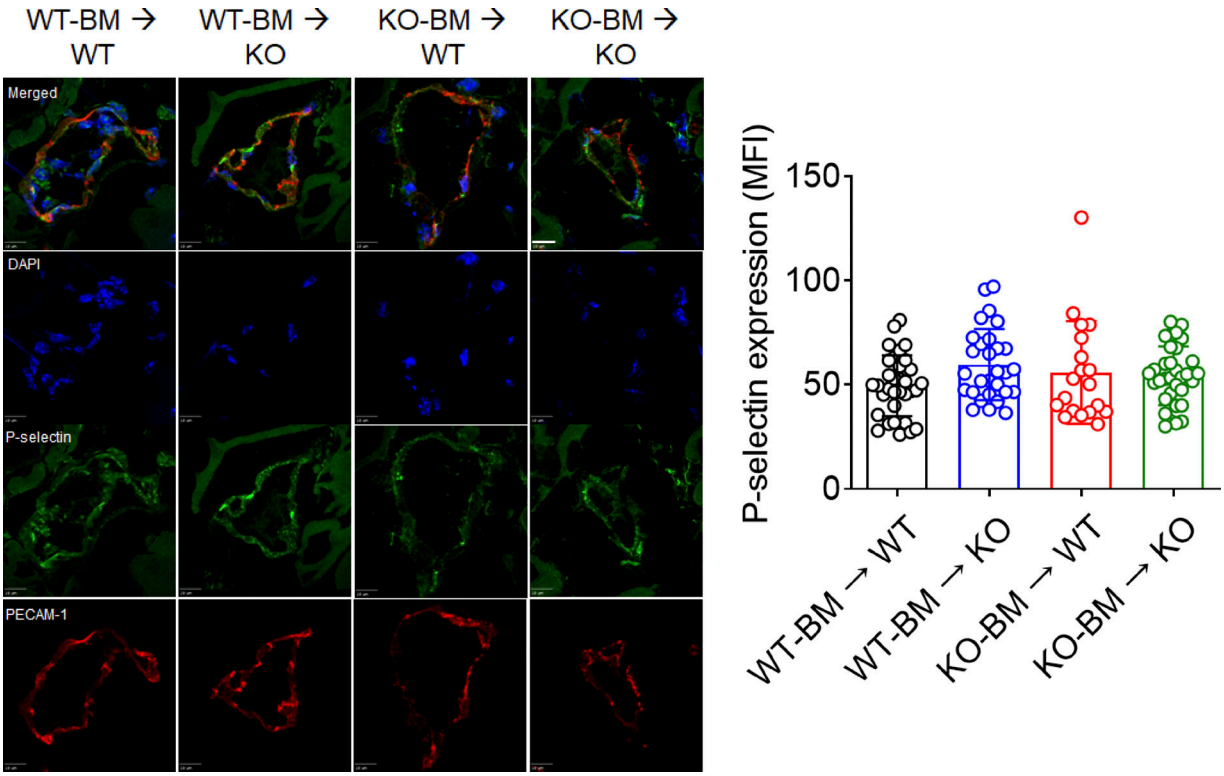


Figure S1. **DREAM deletion does not affect P-selectin expression on the TNF-α–inflamed endothelium.** After intravital microscopy, cremaster muscle in each mouse was removed and sectioned for immunohistochemistry. Tissue sections were stained for P-selectin, PECAM-1, and DAPI, and subjected to confocal microscopy. The MFI values of anti–P-selectin antibodies were quantified. Data represent the mean ± SD ($n$ = 19–33 sections in four mice/group). Scale bar, 10 µm.

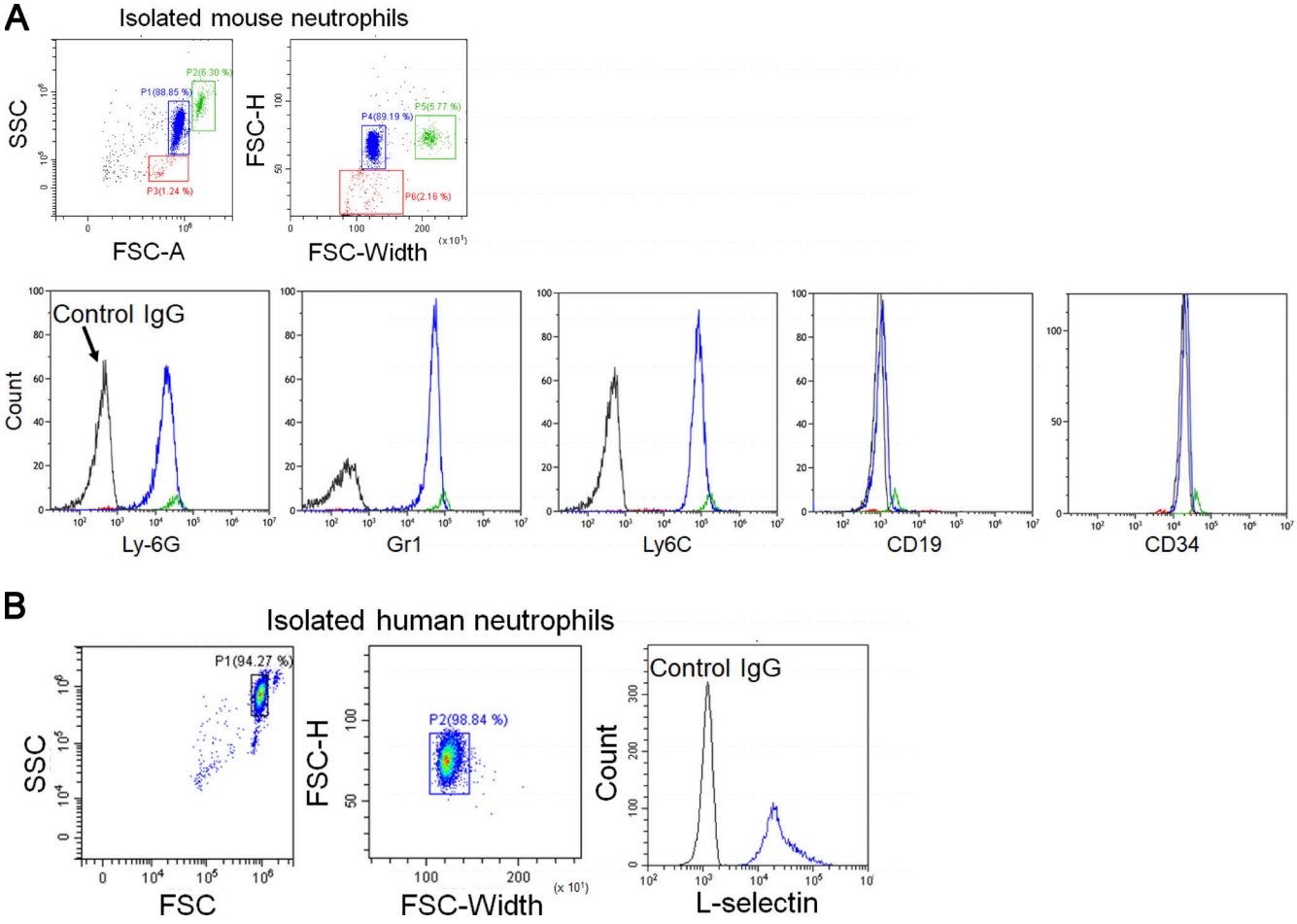


Figure S2. **The purity of isolated mouse and human neutrophils. (A and B)** BM-derived mouse neutrophils (A) and peripheral human neutrophils (B) were analyzed by flow cytometry. The representative data were obtained from three independent experiments. SSC, side scatter; FSC-A, forward scatter area; FSC-H, forward scatter height.

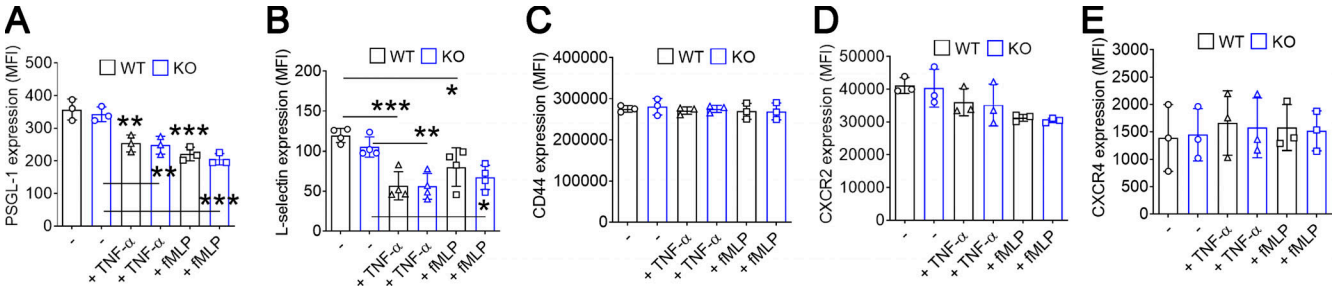


Figure S3. **The expression of surface molecules in WT and DREAM KO neutrophils.** WT and KO neutrophils were treated with or without 5 ng/ml TNF-α or 3 µM fMLP for 10 min. The surface molecules were detected in flow cytometry (mean ± SD, $n$ = 3). *, P < 0.05; **, P < 0.01; ***, P < 0.001 versus unstimulated control (–), ANOVA and Dunnett's test.

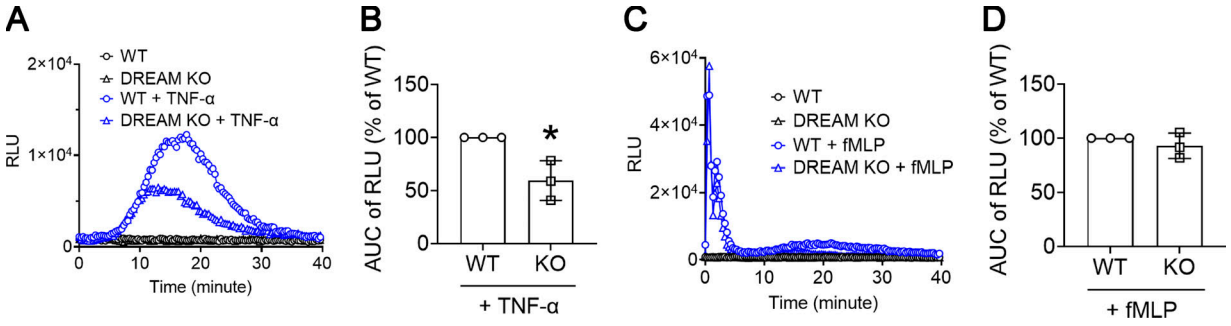


Figure S4. **Neutrophil DREAM positively regulates ROS production in neutrophils stimulated with TNF-α but not fMLP.** WT and DREAM KO neutrophils were adhered to Fg-coated surfaces and then incubated with luminol and horseradish peroxidase. After the addition of 20 ng/ml TNF-α or 10 µM fMLP, light emission was recorded every 20 s at 37°C for 40 min. **(A and C)** A representative trace of ROS production. RLU, relative light unit. **(B and D)** The quantification graph is shown as area under the curve (AUC) of RLU. Mean ± SD ($n$ = 3). *, P < 0.05 versus WT, Student's $t$ test.

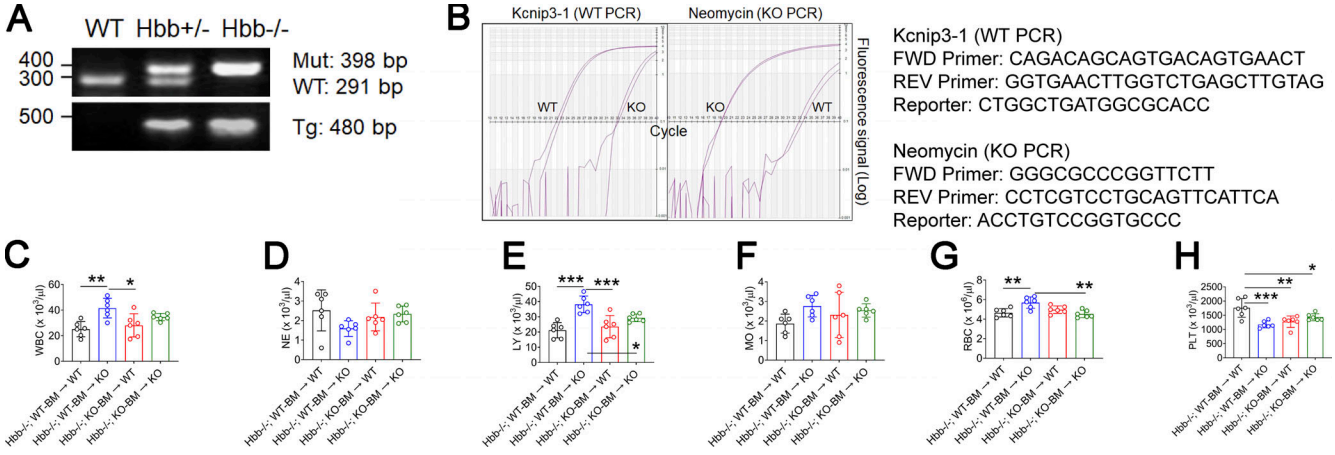


Figure S5. **Genotyping and complete blood counts of SCD mice and nonhematopoietic and/or hematopoietic DREAM-deficient SCD mice.** SCD ($Hbb^{-/-}$) mice deficient in nonhematopoietic and/or hematopoietic DREAM were generated by transplantation of BM cells from SCD mice and DREAM-deficient SCD mice into irradiated WT and DREAM KO mice. **(A and B)** SCD and DREAM KO SCD mice were verified by PCR and RT-qPCR. **(C–H)** Blood cells from mice were counted (mean ± SD, $n$ = 6 mice per group). WBC, white blood cells; NE, neutrophils; LY, lymphocytes; MO, monocytes; PLT, platelets. *, P < 0.05; **, P < 0.01; ***, P < 0.001 after ANOVA and Tukey's test. FWD, forward; REV, reverse; Mut, mutant ($Hbb^{-}$); Tg, transgene.

Video 1. **Neutrophil recruitment during TNF-α–induced cremaster venular inflammation in WT mice.** Neutrophils were monitored by Alexa Fluor 647–conjugated anti-mouse Ly-6G antibody.

Video 2. **Neutrophil recruitment during TNF-α–induced cremaster venular inflammation in DREAM KO mice.** Neutrophils were monitored by Alexa Fluor 647–conjugated anti-mouse Ly-6G antibody.

Video 3. **Recruitment of WT and DREAM KO neutrophils during TNF-α–induced cremaster venular inflammation.** WT (CD45.1) and DREAM KO neutrophils (CD45.2) were monitored by Alexa Fluor 488–conjugated anti-CD45.1 and Alexa Fluor 647–conjugated anti-CD45.2 antibodies, respectively, along with PE-conjugated anti–Ly-6G antibodies. WT neutrophils: $CD45.1^{+}$/$Ly\text{-}6G^{+}$ (cyan) and DREAM KO neutrophils: $CD45.2^{+}$/$Ly\text{-}6G^{+}$ (purple).

Video 4. **Recruitment of WT neutrophils on a monolayer of TNF-α–inflamed ECs.** WT neutrophils were perfused over TNF-α–treated mouse pulmonary vein ECs.

Video 5. **Recruitment of DREAM KO neutrophils on a monolayer of TNF-α–inflamed ECs.** DREAM KO neutrophils were perfused over TNF-α–treated mouse pulmonary vein ECs.

Video 6. **Neutrophil–platelet interactions during TNF-α–induced cremaster venular inflammation in WT mice.** Neutrophils and platelets were monitored by Alexa Fluor 647–conjugated anti–Ly-6G and DyLight 488–conjugated anti-CD42c antibodies, respectively.

Video 7. **Neutrophil–platelet interactions during TNF-α–induced cremaster venular inflammation in DREAM KO mice.** Neutrophils and platelets were monitored by Alexa Fluor 647–conjugated anti–Ly-6G and DyLight 488–conjugated anti-CD42c antibodies, respectively.

**Tables S1–S3 are provided online as separate files. Table S1 shows the number of circulating blood cells in WT and DREAM KO mice. Table S2 shows the number of circulating blood cells in control and DREAM BM chimeric mice. Table S3 shows RNA-seq data of WT and DREAM KO neutrophils following TNF-α stimulation. WT and DREAM KO neutrophils were treated without or with TNF-α for 30 or 120 minutes (*n* = 3). RNA-seq was performed as described in Materials and methods. GSEA shows the gene expression in WT and KO neutrophils.**